# 20 Novel Fluorophores

In the previous chapters we discussed small organic fluorophores typified by the Dansyl, fluorescein, rhodamine, and cyanine dyes. Numerous probes of this type have been characterized and are commercially available. The majority of these probes have extinction coefficients ranging from 10,000 to 100,000 $M^{-1}$ $cm^{-1}$ and decay times ranging from 1 to 10 ns. Some of these probes are photostable, but all the organic fluorophores display some photobleaching, especially in fluorescence microscopy with high illumination intensities. We now describe different types of luminophores that are mostly inorganic or display unusually long lifetimes. These classes of probes are semiconductor nanoparticles, lanthanides, and transition metal–ligand complexes (MLCs). We occasionally use the term luminophore, especially with the MLCs, because it is not clear if the emission occurs from a singlet or triplet state, but we will mostly use the term fluorescent to describe the emission from any of these species.

## 20.1. SEMICONDUCTOR NANOPARTICLES

Starting in 1998[1] there has been rapid development of fluorescent semiconductors nanoparticles. The main component of these particles is usually cadmium selenide (CdSe), but other semiconductors are also used. Particles of CdS, CdSe, InP, and InAs with diameters ranging from 3 to 6 nm can display intense fluorescence. Perhaps the best way to introduce the semiconductor nanoparticles (NPs) or quantum dots (QDots) is by their visual appearance. Figure 20.1 shows a color photograph of suspensions of NPs with different sizes.[2] These are core–shell NPs where the core is CdSe and the shell is ZnS. Another photograph of NPs with different sizes can be found in Figure 21.47. A wide range of emission wavelengths is available by changing the size or chemical composition of the NPs (Figure 20.2). The range of emission wavelengths has been extended to 4 μm using PbSe particles.[3] PbSe QDots with emission wavelengths near 2 μm display quantum yields as high as 25%.

Studies of luminescent NPs first appeared in the early 1980s.[4–7] At that time the quantum yields were low. The NPs were chemically and photochemically unstable and had a heterogeneous size distribution. Since that time there have been many advances in synthesis of homogeneous and stable NPs.[8–11] The chemical and optical properties of NPs have been described in many reviews.[12–16] Figure 20.3 shows a schematic of a typical QDot. Chemical and photochemical stability are improved by coating the CdSe core with a material that has a higher bandgap. The bandgap of a semiconductor is the energy of the longest-wavelength absorption. ZnS has a higher bandgap than CdSe, which means the long-wavelength absorption of ZnS is at a shorter wavelength than CdSe.

The optical properties of NPs are similar to a quantum mechanical particle in a box. Absorption of light results in creation of an electron–hole pair. Recombination of the pair can result in emission. The energy of the excited state decreases as the particle size increases. The energy of the excited state also depends on the material. The use of a higher bandgap shell confines the excited state to the center of the particle. This prevents interactions with the surface that decrease the quantum yield and chemical stability. In order to use the NPs in biological systems they need to be water soluble, which is accomplished with a polymer or silica layer. This layer is then used to attach proteins or nucleic acids.

Several different methods are used to make the NPs biocompatible and to introduce binding specificity.[17–20] The surfaces can be coated with sulfhydryl groups using molecules like mercaptoacetic acid or dihydrolipoic acid, followed by crosslinking to amino groups on the biomolecules (Figure 20.4). NPs have also been coated with silica, for which the surface chemistry is well known. Biomolecules

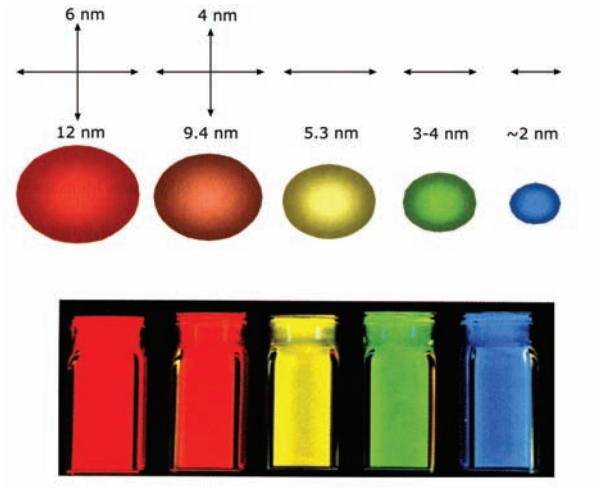


**Figure 20.1**. Color photographs of cadmium selenide nanoparticles illuminated with a long-wave UV lamp. Revised from [2].

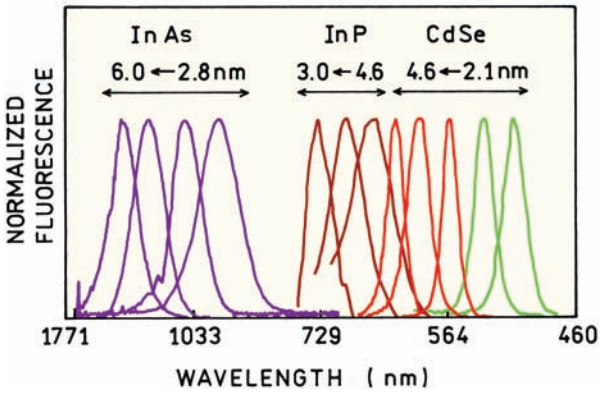


**Figure 20.2**. Emission spectra of semiconductor nanoparticles. The approximate diameters are labeled on the figure. These are core–shell particles. For CdSe the shell is ZnS or CdS. Revised from [1].

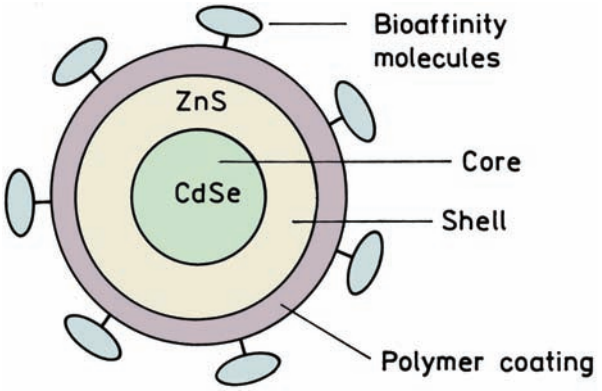


**Figure 20.3**. Schematic of a core–shell NPs with a biologically compatible surface.

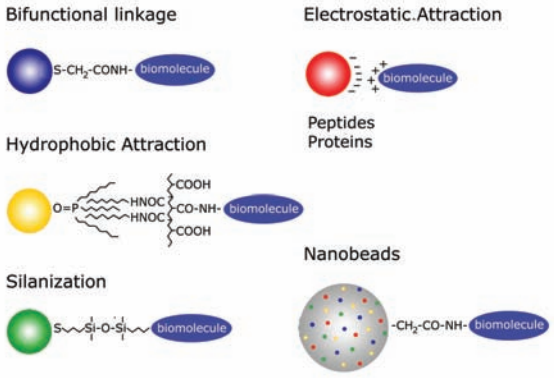


**Figure 20.4**. Methods used to attach biomolecules to NPs. Revised from [20].

can also be bound to the surface by hydrophobic or electrostatic interactions. Using these procedures NPs have been coated with avidin and antibodies. Avidin, which is positively charged, binds spontaneously to negatively charged QDots.[18] When using NPs as probes it is useful to visualize their size.[21] NPs are comparable in size to modest size proteins (Figure 20.5), larger than GFP and smaller than IgG. NPs are much larger than standard fluorophores.

### 20.1.1. Spectral Properties of QDots

QDots display several favorable spectral features. The emission spectra of homogeneously sized QDots are about twofold more narrow than typical fluorophores.[22] This feature can be seen by comparing the emission spectra of cyanine dyes with QDots (Figure 20.6). Additionally, the QDots do not display the long-wavelength tail common to all fluorophores. These tails interfere with the use of multiple fluorophores for imaging or multi-analyte measurements. The emission spectra of the QDots are roughly symmetrical on the wavelength scale and do not display such tails. For this reason the QDots are being used for optical bar codes for multiplexed assays.[23–24] This approach is shown in Figure 20.4 (lower right), which shows a polymer bead containing QDots with different emission wavelengths. See also Section 21.6.

An important spectral property of the QDots is their absorption at all wavelengths shorter than the onset of the absorption.[22] Many of the commonly used organic fluorophores display strong long-wavelength absorption, but

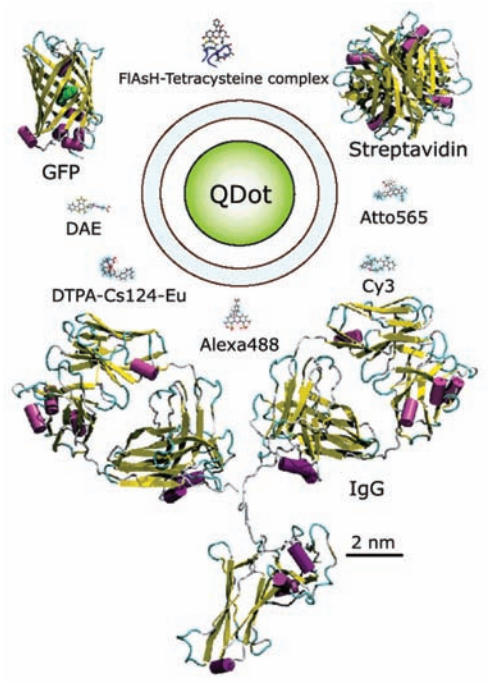


**Figure 20.5**. Relative sizes of luminescent probes and some biomolecules. Revised from [21].

much less absorption at shorter wavelengths. For example, Cy3 and Cy5 are essentially non-absorbing at 400 nm (Figure 20.6). In contrast, the QDots absorb at these shorter wavelengths. This spectral property allows excitation of a range of NP sizes using a single light source, which is needed for practical multiplex assays. The wide absorption spectra also allow excitation with a spectrally wide light source.

The QDots also have large extinction coefficients (ε) that on a molar basis can be up to tenfold larger than rhodamine.[25–26] Small QDots have ε values similar to that of R6G, near 200,000 $M^{-1}$ $cm^{-1}$. Larger QDots can have ε values as large as 2 x $10^6$ $M^{-1}$ $cm^{-1}$. And, finally, QDots can be highly photostable (below), making them useful probes for fluorescence microscopy.

### 20.1.2. Labeling Cells With QDots

Quantum dots are relatively large, and cadmium is toxic, so it was not known if they would be useful for cell labeling. QDots can be cytotoxic under some conditions,[27–28] but it seems that the core–shell particles are nontoxic. Quantum dots covered with mixtures of n-poly(ethylene glyco)phosphatidylethanolamine (PEG-PE) and phosphatidylcholine

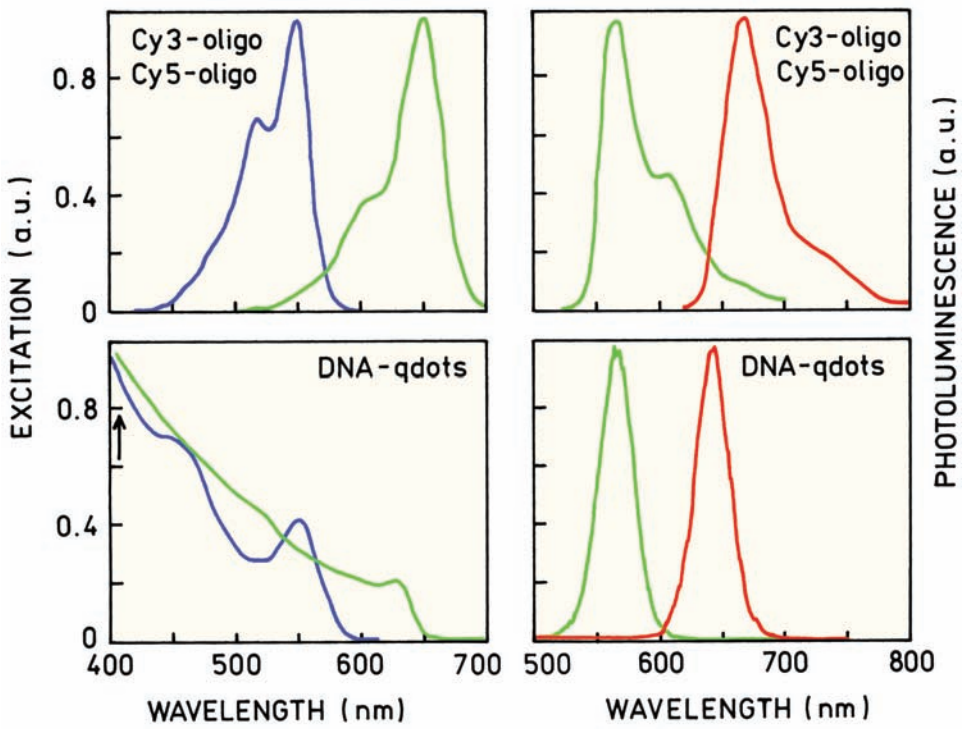


**Figure 20.6**. Absorption and emission spectra of Cy3- and Cy5-labeled oligomers and QDots with bound oligomers. Reprinted with permission from [22]. Copyright © 2003, American Chemical Society.

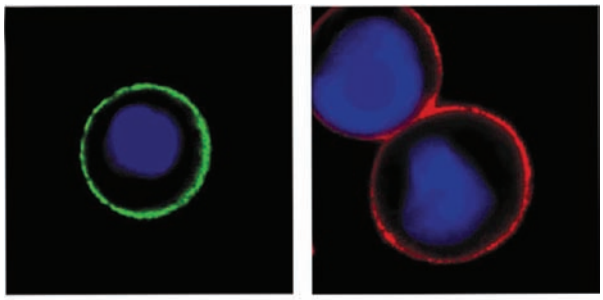

**Figure 20.7**. Labeling of the Her2 marker on breast cancer cells using QDots emitting at 535 (left) or 630 nm (right). From [30].

(PC) were injected into *Xenopus* embryos, with no effect on their development.[29]

QDots can be used for specific labeling of fixed and live cells.[30–31] Her2 is a cancer marker that is overexpressed on the surface of some breast cancer cells. Fixed cells were incubated with monoclonal antibodies against the external domain of Her2. QDots emitting at 535 nm or 630 nm were conjugated to anti-IgG antibodies. These protein-coated antibodies bound specifically to the Her2 markers (Figure 20.7).

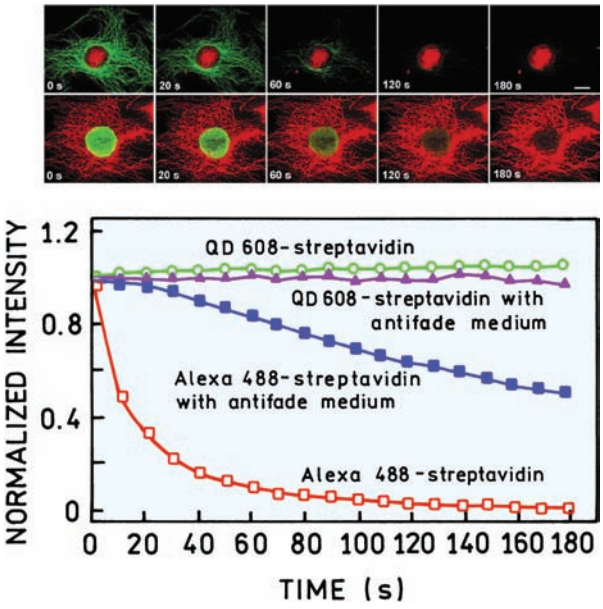


**Figure 20.8**. Photostability comparison between QDots and Alexa 488. Top row: the nuclear antigens were labeled with 630-nm QDots and the microtubules with Alexa 488. Second row: the microtubules were labeled with 630-nm QDots and the nuclear antigens with Alexa 488. The graph shows the intensities with continuous illumination. From [30].

An important property of the QDots is their photostability. Figure 20.8 shows cells labeled with both QDots and the photostable fluorophore Alexa 488. In the top row of images the QDots were localized in the nucleus. In the bottom row of images the QDots were bound to the microtubules in the cytoplasm. These images show that the signal from Alexa 488 is quickly bleached but the QDots remain fluorescent. These results also show that it is possible to label internal cellular structures with QDots and that the intracellular QDots can be highly photostable.

### 20.1.3. QDots and Resonance Energy Transfer

QDots appear to behave like any other fluorophore with regard to energy transfer. RET occurs between QDots.[32–39] The schematic in Figure 20.9 shows a system used to test for RET from a CdSe QDot to a rhodamine acceptor. The QDot surface was coated with biotinylated BSA. Addition of streptavidin labeled with tetramethylrhodamine (SAv-TMR) resulted in quenching of the QDot emission.

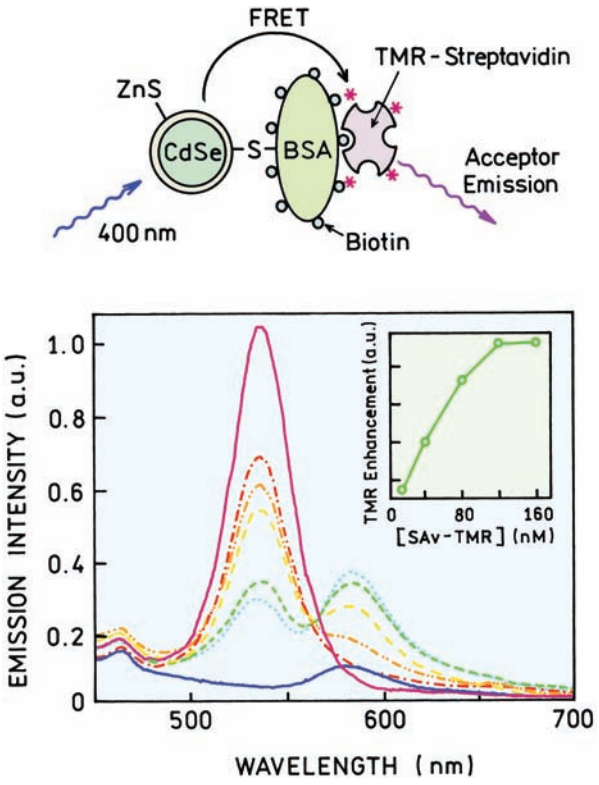


**Figure 20.9**. RET from CdSe QDots to tetramethylrhodamine. The QDot donor intensity decreased (top to bottom at 540 nm) as the concentration of TRM-streptavidin increased. Reprinted with permission from [39]. Copyright © 2001, American Chemical Society.

## 20.2. LANTHANIDES

The lanthanides europium ($Eu^{3+}$) and terbium ($Tb^{3+}$) are unique fluorescent probes. In contrast to all fluorophores described so far these lanthanides display line spectra from the individual atoms. The emission lifetimes of $Eu^{3+}$ and $Tb^{3+}$ are on the millisecond timescale and arise from transitions between the *f* orbitals. The emission rates are low because the transitions are formally forbidden. The inner shell *f* orbital electrons are shielded from the environment, so that lanthanides do not display polarity-dependent spectral shifts and are not quenched by oxygen.

The use of lanthanides in biochemistry originated with their use as a luminescent substitute for calcium.[40–42] Fluorescent probes are usually sensitive to the surrounding environment. The lanthanides can be sensitive to their environment, but in ways different from typical fluorophores. The decay times of the lanthanides depend on the number of coordinated water molecules.[43–45] The number of bound water molecules ($n$) is given by

$$n = q\left(\frac{1}{\tau_{H_2O}} - \frac{1}{\tau_{D_2O}}\right) \qquad (20.1)$$

where the lifetimes are measured in $H_2O$ and $D_2O$. The values of $q$ are 1.05 and 4.2 for $Eu^{3+}$ and $Tb^{3+}$, respectively. The lanthanides can bind to proteins in place of calcium and the lifetimes can be used to determine the hydration of the protein-bound ions. The lanthanide decay times can also be affected by RET. Since the lanthanides have low extinction coefficients they are not useful as acceptors. However, the lanthanides can have high quantum yields and can serve as donors. At present most applications of the lanthanides are based on their use as RET donors.

Because of their low extinction coefficients the lanthanides are not usually excited directly. The ions are at first bound to chelators that contain a fluorophore (Figure 20.10). The energy from the fluorophore can be efficiently transferred to the lanthanide. The energy of the excited fluorophore must be adequate to excite the lanthanide. The chelators serve two other purposes. The chelator increases the quantum yield of the lanthanide by displacing the bound water molecules that act as quenchers. The chelator also provides a means to bind the lanthanide to a biomolecule using standard coupling chemistry. A large number of chelators have been described.[46–48] The more recent papers often describe chelators that are conjugatable or otherwise designed for biological applications.[49–54] However, many of these chelators are not commercially available. The need to synthesize suitable chelators appears to limit the use of lanthanides in biochemical research.

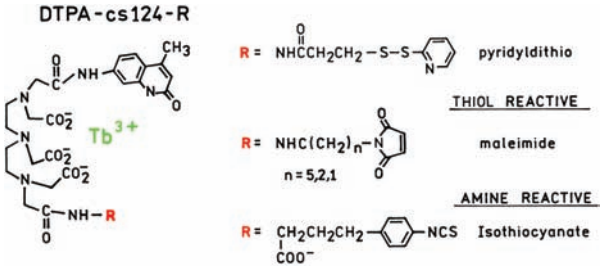


**Figure 20.10**. Conjugatable chelators for lanthanides. Reprinted with permission from [46]. Copyright © 1999. With kind permission of Springer Science and Business Media.

Figure 20.11 shows the emission spectra and intensity decays of $Tb^{3+}$ and $Eu^{3+}$ when complexed with DTPA-cs124. These emission spectra show no component from the carbostyril 124, which is part of the chelator. These spectra were recorded using a light chopper with a 145-μs delay to suppress the prompt fluorescence from carbostyril 124. It is possible to use such long time delays because of the 0.61- and 1.54-ms lifetimes of the $Eu^{3+}$ and $Tb^{3+}$ chelates, respectively. If the spectra were recorded without time-delayed

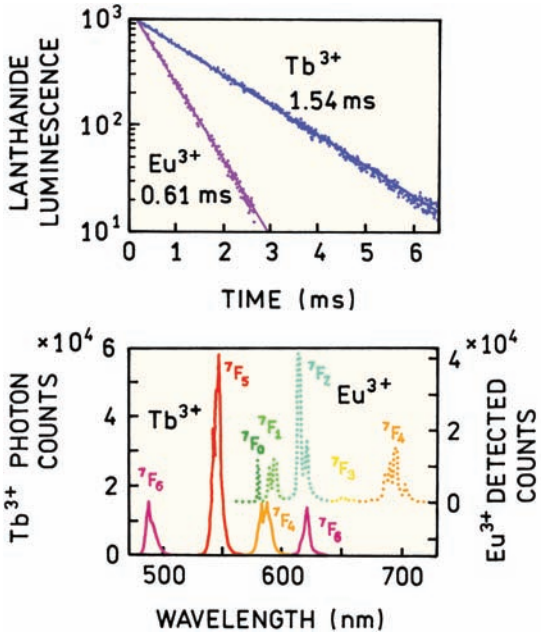


**Figure 20.11**. Emission spectra and intensity decays of $Tb^{3+}$ and $Eu^{3+}$ complexed with DTPA-cs124. Emission from $Tb^{3+}$ in $^5D_4 \rightarrow {}^7Fj$ and from $Eu^{3+}$ in $^5D_0 \rightarrow {}^7Fj$. Reprinted with permission from [46]. Copyright © 1999. With kind permission of Springer Science and Business Media.

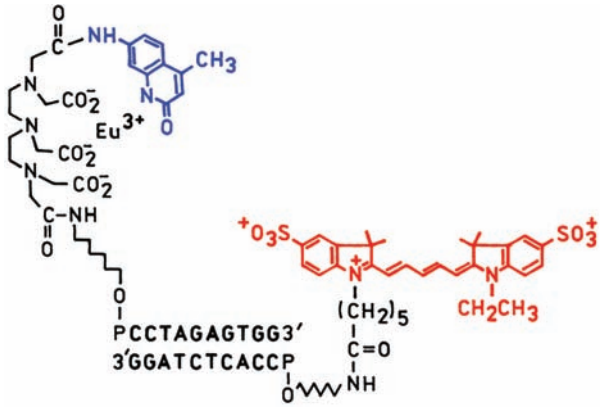


**Figure 20.12**. Lanthanide–cyanine donor–acceptor pair linked by a DNA oligomer. Revised and reprinted with permission from [57]. Copyright © 1994, American Chemical Society.

detection there would probably be a large contribution from carbostyril 124, which would be due to DTPA-cs124 without bound lanthanide.

### 20.2.1. RET with Lanthanide

Lanthanides have a number of favorable properties as RET donors.[46,55–57] The value of $R_0$ are typically 50–70 Å for transfer from chelated lanthanides. The Förster distances can be as large as 90 Å for transfer to allophycocyanine. The quantum yields of lanthanide chelates depend on the concentration of water, so that the quantum yield and the value of $R_0$ can be adjusted to some degree using the $H_2O/D_2O$ mixture. The emission from lanthanides is unpolarized so there is less concern with $\kappa^2$, which must be between 1/3 and 4/3 for the most extreme cases. This range of $\kappa^2$ values can result in a maximum error in the distance of only 12%. The long decay times make it possible to measure the decays with high precision and with suppression of background. And, finally, use of the long-lived acceptor emission allows selective observation of only the D–A pairs without observing free donor or free acceptor.

Figure 20.12 shows an example of RET from a chelated lanthanide to a Cy5 acceptor. The donor and acceptor are linked to opposite ends of a DNA oligomer.[55–56] The emission spectrum for the D–A pair shows the expected europium emission spectrum and emission from Cy5 centered near 668 nm (Figure 20.13). This component was not due to directly excited Cy5 because the emission spectra were collected with a time delay of 90 µs and the decay time of directly excited Cy5 is close to 1 ns. The intensity decay of the donor alone is a single exponential. The donor decay in

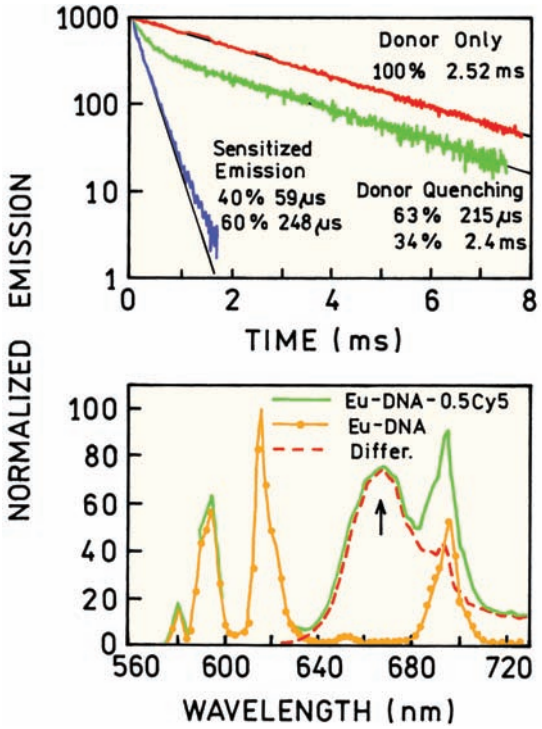


**Figure 20.13**. Emission spectra and intensity decays of the donor–acceptor pair shown in Figure 20.12. The emission spectra were collected with a time delay of 90 µs. The intensity decays were measured for the donor at 617 nm and for the sensitized acceptor emission at 668 nm. Reprinted with permission from [46]. Copyright © 1999. With kind permission of Springer Science and Business Media.

the D–A pair shows two decay times: 0.22 and 2.40 ms. The 2.40-ms component is the same decay time as the donor alone and the component is due to donor strands of DNA that are not hybridized with acceptor strands.

A valuable property of lanthanide donor–acceptor pairs is the ability to selectively observe the pairs in the presence of unpaired donors and acceptors. The rapidly decaying component in Figure 20.13 is for the sensitized acceptor emission measured at 668 nm. This acceptor emission is due to energy transfer from the donor, and it decays with the same rate as the donor. Hence the decay time of this component (0.22 ms) represents the decay time of the donor in D–A pairs. Selective observation of this component is possible because of the structured emission of the donor that does not emit at the maximum of the acceptor emission. The 59-µs component in the sensitized acceptor emission is due to an artifact in the detector.

There are several aspects of RET with lanthanide donors that are worthy of mention. RET occurs due to dipolar

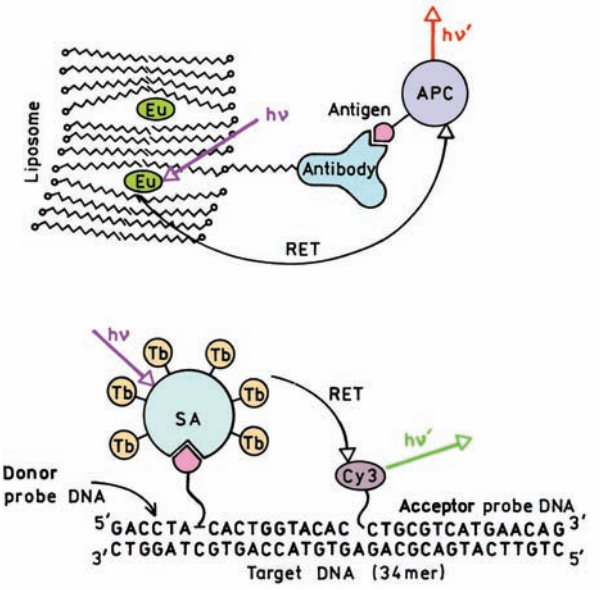


**Figure 20.14**. Schematic of an immunoassay and a DNA assay using RET with a lanthanide donor. APC, allophycocyanine; B, biotin; SA, streptavidin. The chelators are not shown. Revised from [58–59].

interactions. The two shorter wavelengths transitions around 590–600 nm for europium are thought to be magnetic dipoles and are not included in calculation of the overlap integrals. The intensity decay of the sensitized acceptor, and thus also that of the donor, are single exponentials. This is somewhat surprising because the flexibility of the linkers (Figure 20.12) is expected to result in a distribution of donor-to-acceptor distances. Any effect of a distance distribution is probably eliminated due to diffusive motions during the donor lifetime (Sections 15.5 and 15.6). It is also interesting to notice that RET from a lanthanide donor occurs on a millisecond timescale, whereas RET from a nanosecond donor occurs on a nanosecond timescale. This dependence on the decay time of the donor is because the transfer rate is proportional to the radiative decay rate of the donor (Section 13.2).

In Section 3.9.1 we described the use of lanthanides with gated detection for high-sensitivity assays. The detector is gated on after the prompt autofluorescence has decayed. With gated detection the goal is not to measure distances but rather to obtain the highest possible sensitivity. Figure 20.14 shows examples of DNA hybridization assays and immunoassays using lanthanides and RET.[58–59] In both cases the signal levels are increased by the use of multiple-lanthanide donors. The immunoassay uses allophycocyanine as the acceptor, which results in large Förster distances due to the high extinction coefficients of the phycobiliproteins. The DNA hybridization assay uses Cy3 as the acceptor.

RET with lanthanides can also be used for structural studies of proteins.[60] One example is tropomyosin that was labeled with a terbium donor and a TMR acceptor on cysteine residues at positions 56 and 100, respectively (Figure 20.15). The shortest component of 0.03 ms is due to a ringing artifact in the gated detector. The decrease in lifetime from 1.37 to 0.61 ms indicates a transfer efficiency of 56%. Based on the Förster distance of $R_0$ = 57 Å, this efficiency indicates a distance of 55 Å. This distance is shorter than the value of 65 Å obtained from the x-ray structure. The smaller recovered distance is probably due to flexing of tropomyosin during the millisecond donor lifetime.

### 20.2.2. Lanthanide Sensors

Because of the shielded *f* orbitals the lanthanides are rather insensitive to their local environment. This makes it difficult to develop analyte-sensitive probes like those available for calcium and other ions (Chapter 19). However, lanthanide-based sensors have been developed using different principles. Lanthanide-based sensors can depend on

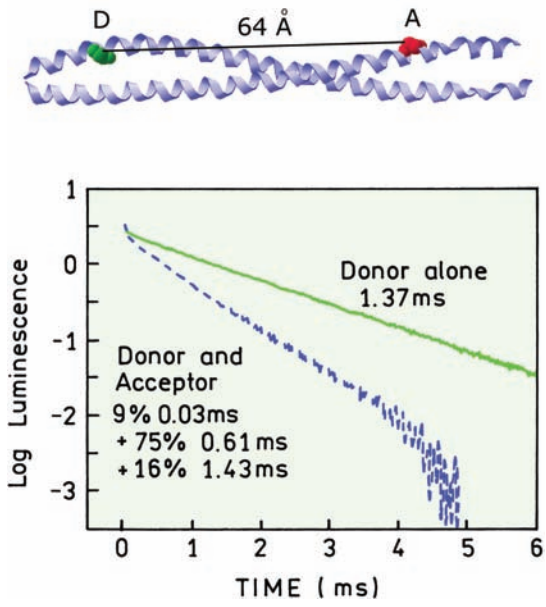


**Figure 20.15**. Intensity decays of tropomyosin labeled with a $Tb^{3+}$ donor, or with both the donor and a TMR acceptor. The chelator was a sulfhydryl-reactive version of DPTA-cs124. Revised and reprinted with permission from [60]. Copyright © 2004, American Chemical Society.

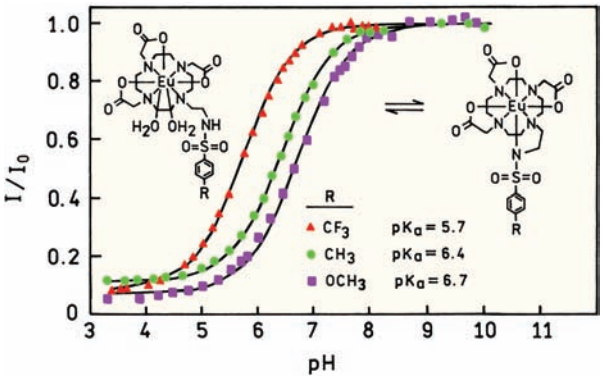


**Figure 20.16**. Lanthanide-based pH sensor. From [66].

changes in hydration or changes in RET from the chelator.[61–67] The lanthanide chelate shown in Figure 20.16 displays an increased intensity at higher pH values. This increase in intensity is due to removal of a bound water molecule that is displaced by the sulfonamide at high pH. Figure 20.17 shows excitation spectra of a cyclodextran terbium complex with increasing concentrations of naphthalene. The increased emission intensity of terbium at 544 nm is due to energy transfer from naphthalene as it binds in the cyclodextran cavity.

### 20.2.3. Lanthanide Nanoparticles

The long lifetime and large Stokes shift of the lanthanides make them useful in high-sensitivity assays. The sensitivity can be increased using nanoparticles that contain a large number of lanthanide chelates.[68–71] These nanoparticles are just becoming available, and the compositions are likely to evolve. Some of the particles are polystyrene and contain the lanthanide and a hydrophobic chelator. Other preparations are based on silica-coated particles of the chelated lanthanide (Figure 20.18). In both cases the surfaces are derivatized to contain reactive groups for binding to biomolecules.

### 20.2.4. Near-Infrared Emitting Lanthanides

Red-emitting or near-infrared (NIR) emitting fluorophores can be useful for high-sensitivity detection because of the decreased autofluorescence at longer wavelengths. NIR-emitting lanthanides are also known. Erbium (Er), neodymium (Nd), and ytterbium (Yb) emit at wavelengths ranging from 900 to 1500 nm (Figure 20.19).[72–74] Because of their longer-wavelength absorption spectra these lanthanides can be sensitized by longer-wavelength fluorophores like fluorescein and eosin,[73] and even by an NIR fluorophore absorbing at 980 nm.[75] The spectra shown in Figure 20.19 were recorded with excitation at 488 nm, where these fluorophores absorb. At present, the quantum yield of the NIR lanthanides are low. However, there are ongoing efforts to synthesize chelators that result in higher quantum yields from the NIR lanthanides.[76–77] The NIR lanthanides are beginning to find a use in immunoassays.[78]

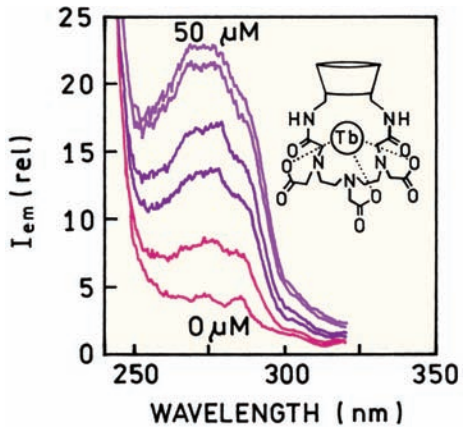


**Figure 20.17**. Excitation spectra of a cyclodextran terbium complex with increasing concentrations of naphthalene. Excitation at 275 nm and emission at 544 nm. Revised and reprinted with permission from [67]. Copyright © 1996, American Chemical Society.

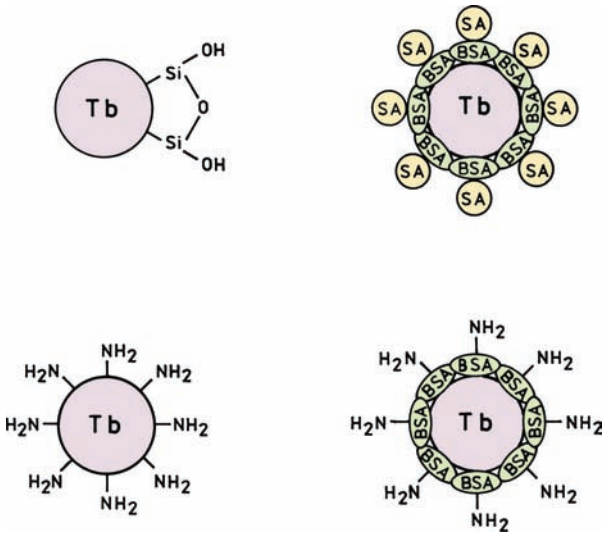


**Figure 20.18**. Lanthanide-containing nanoparticles. The particles are about 42 nm in diameter. Revised and reprinted with permission from [71]. Copyright © 2004, American Chemical Society.

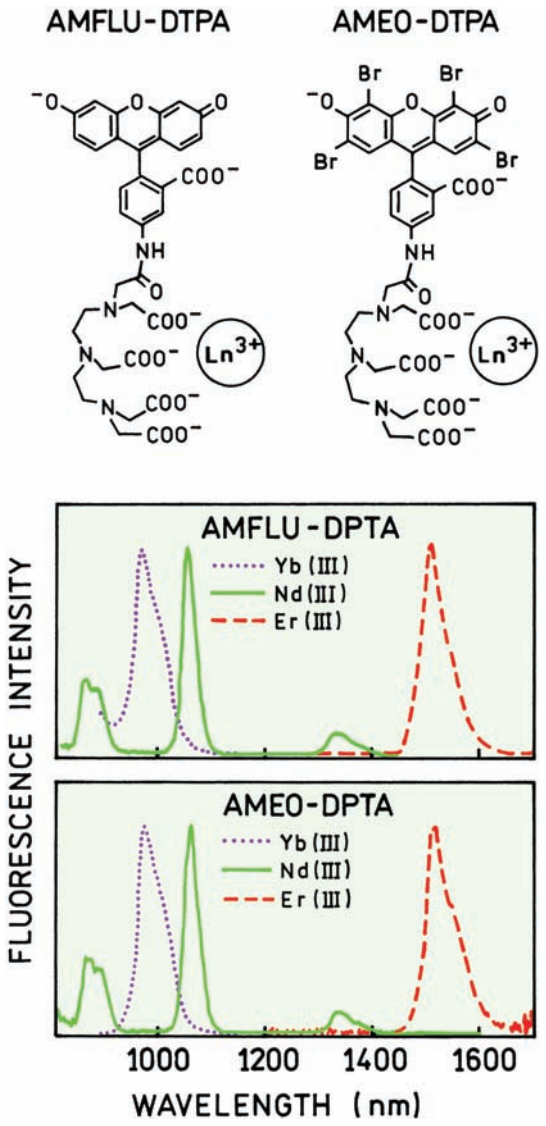


**Figure 20.19**. Emission spectra of NIR-emitting lanthanide chelators. Excitation at 488 nm. Revised from [72].

### 20.2.5. Lanthanides and Fingerprint Detection

Detection and imaging of fingerprints is often performed in a crime-scene investigation (CSI). Fingerprints are often detected with colorimetric or fluorogenic reagents that react with amino groups.[79–80] Lanthanides can also be used for visualization of fingerprints.[81–83] Detection is based on the quenching of lanthanides by water. Fingerprints are often treated with cyanoacrylate, which reacts with molecules in the prints. These treated prints can be sprayed by a lanthanide chelate that has several bound water molecules. The chelator is usually hydrophobic. The chelator with its bound lanthanide partitions into the polymer and/or fingerprints. When this occurs the water is left behind and the lanthanides become more brightly fluorescent. The large Stokes shift and narrow emission spectra of the lanthanides allows for effective use of filters to remove the incident light and unwanted background fluorescence.

## 20.3. LONG-LIFETIME METAL–LIGAND COMPLEXES

Organic fluorophores have decay times ranging from 1 to 20 ns and lanthanides have millisecond decay times. These timescales are useful for many biophysical measurements, but there are numerous instances where intermediate decay times are desirable. For instance, one may wish to measure rotational motions of large proteins or membrane-bound proteins. In such cases the overall rotational correlation times can be near 200 ns, and can exceed 1 μs for larger macromolecular assemblies. Rotational motions on this timescale are not measurable using fluorophores that display ns lifetimes. Processes on the μs or even the ms timescale have occasionally been measured using phosphorescence.[84–86] However, relatively few probes display useful phosphorescence in room temperature aqueous solutions. Also, it is usually necessary to perform phosphorescence measurements in the complete absence of oxygen. The lanthanides are not quenched by oxygen, but their emission is not polarized so they are not useful for measurements of rotational diffusion. Also, the millisecond lanthanide lifetimes are too long for measurements of many dynamic processes. Hence, there is a clear need for probes that display microsecond lifetimes. In this section we describe a family of metal–ligand probes that display decay times ranging from 100 ns to 10 μs. The long lifetimes of the metal–ligand probes allow the use of gated detection, which can be used to suppress interfering autofluorescence from biological samples and thus provide increased sensitivity.[87] And, finally, the metal–ligand probes display high chemical and photochemical stability and are reasonably soluble in water. Because of these favorable properties, metal–ligand probes can have numerous applications in biophysical chemistry, clinical chemistry, and DNA diagnostics.

### 20.3.1. Introduction to Metal–Ligand Probes

The term metal–ligand complex (MLC) refers to transition metal complexes containing one or more diimine ligands. This class of probes is typified by $[Ru(bpy)_3]^{2+}$, where bpy

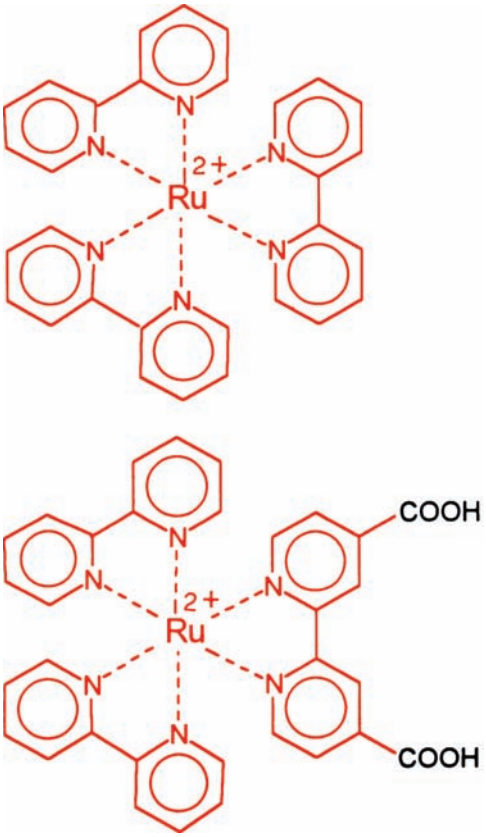


**Figure 20.20**. Chemical structure of $[Ru(bpy)_3]^{2+}$ and of $[Ru(bpy)_2(dcbpy)]^{2+}$. The latter compound is conjugatable and displays strongly polarized emission.

is 2,2'-bipyridine (Figure 20.20). This class of compounds was originally developed for use in solar energy conversion and has become widely used as model compounds to study excited-state charge transfer. Upon absorption of light $[Ru(bpy)_3]^{2+}$ becomes a metal-to-ligand charge-transfer species, in which one of the bpy ligands is reduced and ruthenium is oxidized:

$$Ru^{II}(bpy)_3^{2+} \xrightarrow{h\nu} Ru^{III}(bpy)_2(bpy^-)^{2+} \qquad (20.2)$$

where $Ru^{III}$ is a strong oxidant and $bpy^-$ a strong reductant. It was hoped that this charge separation could be used to split water to hydrogen and oxygen. A wide variety of luminescent MLCs are now known, some of which are strongly luminescent and some of which display little or no emission. The metals are typically rhenium (Re), ruthenium (Ru), osmium (Os), or iridium (Ir). A number of extensive reviews of their spectral properties is available.[88–96]

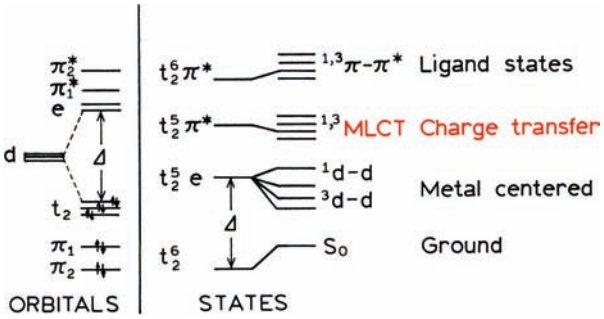


**Figure 20.21**. Orbital and electronic states of metal–ligand complexes. The *d* orbitals are associated with the metal, and are split by energy Δ due to the crystal field created by the ligands. The π orbitals are associated with the ligand. Reprinted with permission from [97]. Copyright © 1994. With kind permission of Springer Science and Business Media.

Prior to discussing the spectral properties of the MLCs, it is useful to have an understanding of their unique electronic states (Figure 20.21). The π orbitals are associated with the organic ligands and the *d* orbitals are associated with the metal. All the transition metal complexes we will discuss have six *d* electrons. The presence of ligands splits the *d*-orbital energy levels into three lower ($t$) and two higher ($e$) orbitals. The extent of splitting is determined by the crystal field strength Δ. The three lower energy *d* orbitals are filled by the six *d* electrons. Transitions between the orbitals ($t \otimes e$) are formally forbidden. Hence, even if *d*–*d* absorption occurs the radiative rate is low and the emission is quenched. Additionally, electrons in the e orbitals are antibonding with respect to the metal–ligand bonds, so excited *d*–*d* states are usually unstable.

The appropriate combination of metal and ligand results in a new transition involving charge transfer between the metal and ligands (Figure 20.22). For the complexes described in this chapter the electrons are promoted from the metal to the ligand, the so-called metal-to-ligand charge

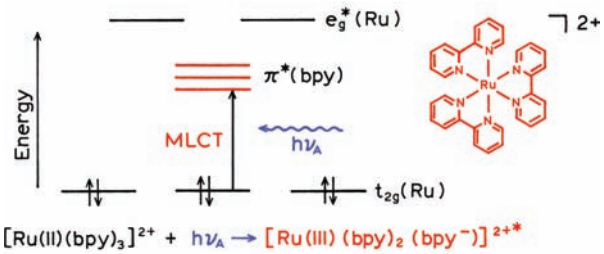


**Figure 20.22**. Metal-to-ligand charge transfer (MLCT) transition in $[Ru(bpy)_3]^{2+}$. From [98].

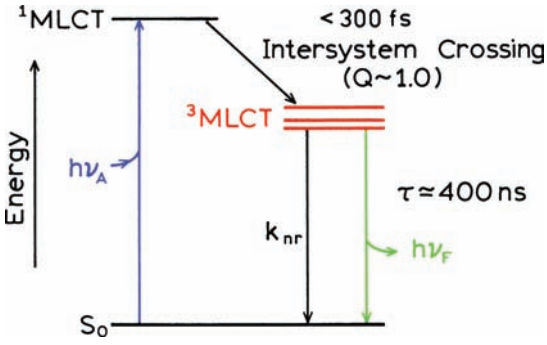


**Figure 20.23**. Jablonski diagram for a metal–ligand complex $[Ru(bpy)_3]^{2+}$. The decay time is near 400 ns.

transfer (MLCT) transition. The MLCT transition is the origin of the absorbance of the ruthenium MLCs near 450 nm. Emission from these states is formally phosphorescence. However, these states are shorter lived (microseconds) than normal phosphorescent states, and thus can emit prior to quenching. The luminescence of MLCs is thought to be short lived due to spin–orbit coupling with the heavy metal atom, which increases the allowedness of the normally forbidden transition to the ground state.

A Jablonski diagram for the metal–ligand complexes is shown in Figure 20.23. Following absorption the complex undergoes intersystem crossing to the triplet MLCT state. This occurs rapidly:[99–102] in less than 300 fs and with high efficiency. Once in the MLCT state the excited-state complex decays by the usual radiative ($\Gamma$) and non-radiative ($k_{nr}$) decay pathways. In general the values of $k_{nr}$ are larger

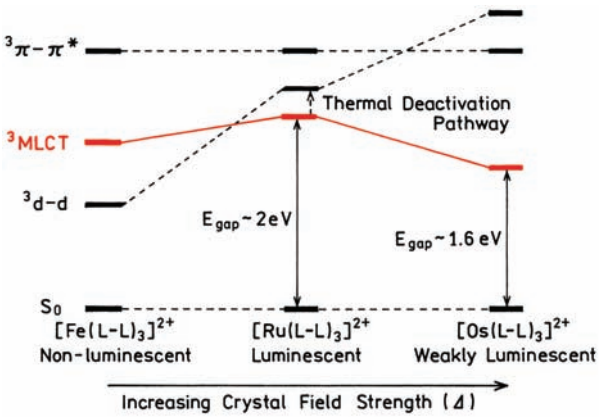


**Figure 20.24**. Lowest energy triplet states for metal–ligand complexes with increasing crystal field strength. Revised and reprinted with permission from [103]. Copyright © 1991, American Chemical Society.

than $\Gamma$, and the decay times are determined mostly by the non-radiative decay rates.

For an MLC to be luminescent several criteria must be satisfied. The crystal field must be strong enough to raise the *d–d* state above the MLCT state. Hence, iron MLCs $[Fe(L\text{-}L)_3]^{2+}$ are non-luminescent due to the low lying *d–d* state (Figure 20.24). In contrast $[Ru(L–L)_3]^{2+}$ is luminescent because the *d–d* states are above the MLCT state and do not serve as a major route of radiationless decay. $[Os(L\text{-}L)_3]^{2+}$ has still higher *d–d* energies. Since the *d–d* levels are not accessible, osmium complexes are highly photostable. However, osmium MLCs are usually weakly luminescent. This is a result of the energy gap law. As the energy of the excited state becomes closer to the ground state, the rate of radiationless decay increases due to the energy gap law. Smaller energy gaps result in more rapid radiationless decay (Section 20.3.4). Osmium MLCs typically have long-wavelength emission, a low-energy MLCT state, and a rapid rate of radiationless decay.

The relative levels of MLCT and *d–d* states determine the sensitivity of the MLC decay times to temperature. If the *d–d* levels are close to the MLCT level, then the *d–d* states are thermally accessible. In such cases increasing temperature results in decreased lifetimes due to thermal population of the *d–d* states, followed by rapid radiationless decay. Osmium complexes with thermally inaccessible *d–d* levels are less sensitive to temperature.[103–104]

### 20.3.2. Anisotropy Properties of Metal–Ligand Complexes

The interest in MLCs as biophysical probes was stimulated by the observation that some MLCs display strongly polarized emission. The structure of $[Ru(bpy)_3]^{2+}$ is highly symmetrical with three identical ligands. Hence, one does not expect the excited state to be localized on any particular ligand, and the emission is expected to display low or zero anisotropy. However, it was found that Ru MLCs that contained nonidentical diimine ligands displayed high anisotropy. The first such compound studied[105] was the dicarboxy derivative $[Ru(bpy)_2(dcbpy)]^{2+}$, where dcpby is 4,4'-dicarboxy-2,2'-bipyridyl (Figure 20.20, right). The excitation anisotropy spectrum of this MLC is shown in Figure 20.25, along with that of several similar RuMLCs. The dicarboxy ligand was conjugated to human serum albumin (HSA) via the carboxyl groups. Higher fundamental anisotropies ($r_0$) were observed for the dicarboxy derivative than for $[Ru(bpy)_3]^{2+}$. Also, usefully high anisotropies were

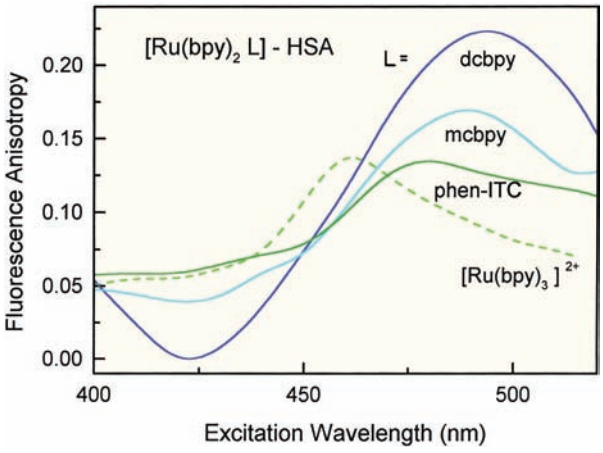


**Figure 20.25**. Excitation anisotropy spectra of $[Ru(dcbpy)(bpy)_2]^{2+}$, $[Ru(mcbpy)(bpy)_2]^{2+}$ and $[Ru(phen\text{-}ITC)\text{-}(bpy)_2]^{2+}$, conjugated to HSA. $[Ru(bpy)_2L]$-HSA in 6:4 (V/V) glycerol/water, T = –55°C. Also shown is the anisotropy spectrum of $[Ru(bpy)_3]^{2+}$ in 9:1 (V/V) glycerol/water, –55°C (dashed).

observed for a number of MLCs (Figure 20.26). A variety of bioconjugatable MLCs have now been described,[106–112] including a biotin-containing MLC.[113] MLC-labeled nucleotides have also been reported.[114–118]

The potential of the MLCs as biophysical probes is illustrated by the range of decay times and quantum yields available with this diverse class of compounds. The chemical structures of useful rhenium (Re), ruthenium (Ru), and osmium (Os) complexes are shown in Figure 20.27. When conjugated to HSA in oxygenated aqueous solution at room temperature, the rhenium MLC display lifetimes as long as 2.7 μs, and up to 4 μs in the absence of oxygen.[119] The osmium complex displays a much shorter lifetime and lower quantum yield,[120] but can be excited at 680 nm. The possibility of long-wavelength excitation and long decay times shows that the MLCs have significant potential as biophysical probes.[121–123]

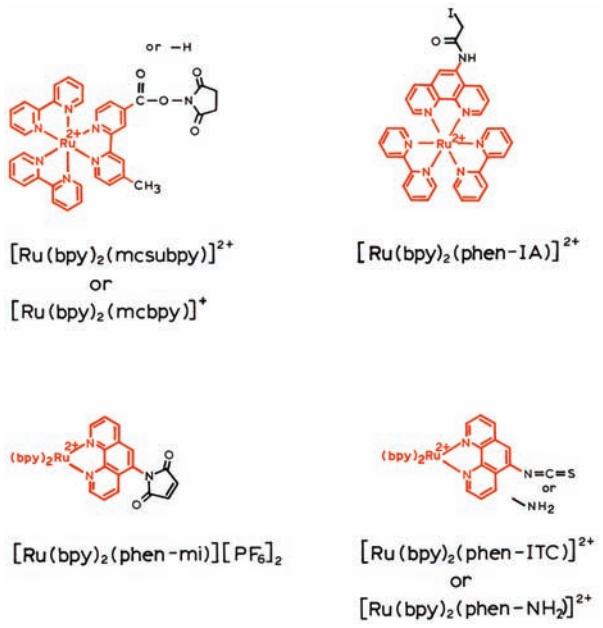


**Figure 20.26**. Conjugatable metal–ligand complexes.

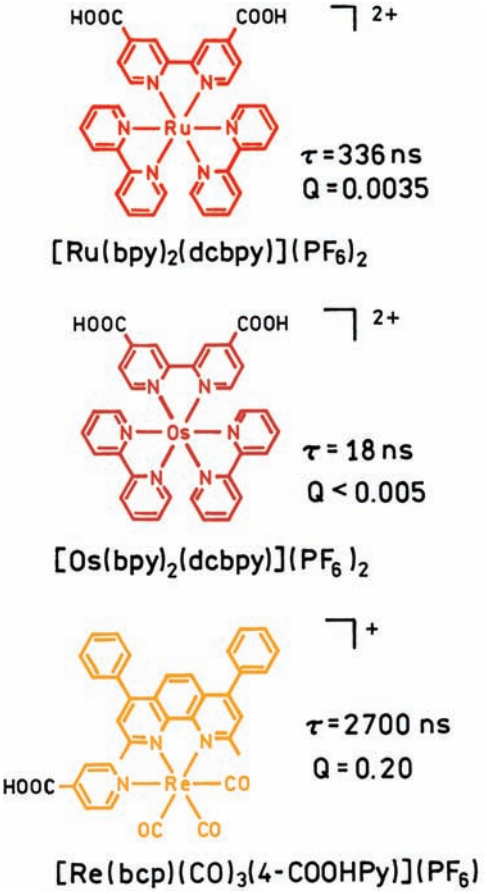


**Figure 20.27**. Chemical structures of ruthenium (II), osmium (II), and rhenium (I) metal–ligand complexes. The decay times and quantum yields are for these compounds covalently linked to human serum albumin. The decays are multi-exponential.

### 20.3.3. Spectral Properties of MLC Probes

The metal–ligand complexes have favorable absorption and emission spectra. Absorption and emission spectra of three conjugatable MLCs are shown in Figure 20.28. The long-wavelength absorption of the Ru MLCs is not due to

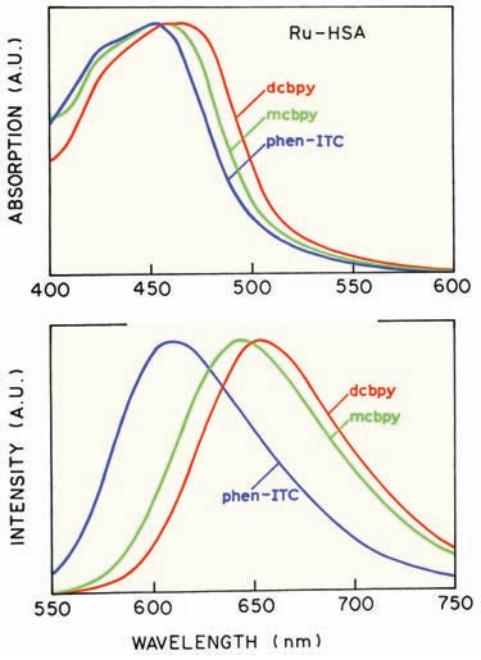


**Figure 20.28**. Absorption and emission spectra of $[Ru(bpy)_2(dcbpy)]^{2+}$, $[Ru(bpy)_2(mcbpy)]^{+}$, and $[Ru(bpy)_2$ phen-ITC$]^{2+}$ conjugated to HSA. Excitation wavelength 460 nm, at 20°C. Structures are shown in Figures 20.26 and 20.27. Revised from [110]. Copyright © 1996, with permission from Elsevier Science.

absorption of the metal alone or the ligand alone. Localized absorption by the ligand, referred to as ligand centered (LC) absorption, occurs at shorter wavelengths near 300 nm. Absorption by the *d–d* transitions of the metal is forbidden and the extinction coefficients are very low (1 to 200 $M^{-1}$ $cm^{-1}$). The broad absorption band at 450 nm is due to the metal-to-ligand charge transfer (MLCT) transition (eq. 20.2). The MLCT transitions display extinction coefficients of 10,000 to 30,000 $M^{-1}$ $cm^{-1}$. These values are not as large as fluorescein or cyanine dyes, but these extinction coefficients are comparable to those found for many fluorophores, and are adequate for some applications.

The emission of the metal–ligand complexes is also dominated by the MLCT transition, which is centered near 650 nm (Figure 20.28) for the Ru(II) complexes. The MLCs behave like a single chromophoric unit. In contrast to the lanthanides, the absorption and emission are not due to the atom, but rather to the entire complex. Also, the metal–ligand bonds are covalent bonds, and the ligands and metal do not dissociate under any conditions that are remotely physiological.

Examination of Figure 20.28 reveals another favorable spectral property of the MLCs, namely a large Stokes shift, which makes it relatively easy to separate the excitation and emission. This large shift results in minimal probe–probe interaction. In contrast to fluorescein, which has a small Stokes shift, the MLCs do not appear to self-quench when multiple MLCs are attached to a protein molecule. Additionally, the MLCs do not appear to be prone to self-association.

For the ruthenium complexes, comparison of Figures 20.25 and 20.28 reveals that the MLCs with the longest emission wavelengths display the highest anisotropy. This behavior seems to correlate with the electron-withdrawing properties of the ligand, which are highest for dcbpy and lowest for phenanthroline isothiocyanate. In general it seems that having one ligand to preferentially accept the electron in the MLC transition results in high fundamental anisotropies. This suggests that MLCs with a single chromophoric ligand will have high anisotropies, which has been observed for Re(I) complexes.[119]

### 20.3.4. The Energy Gap Law

One factor that affects the decay times of the metal–ligand complexes is the energy gap law. This law states that the non-radiative decay rate of a metal–ligand complex increases exponentially as the energy gap or emission energy decreases.[124–130] One example of the energy gap law is shown in Table 20.1 for Re(I) complexes. The structure of these complexes is similar to the lowest structure in Figure 20.27, except that the chromophoric ligand is bpy. In this complex the emission maximum is sensitive to the structure of the non-chromophoric ligand. The radiative decay rates ($\Gamma$) are relatively independent of the ligand but the non-radiative decay rate ($k_{nr}$) is strongly dependent on the ligand and emission maximum. The dependence of $k_{nr}$ on emission energy for a larger number of Re(I) complexes is shown in Figure 20.29. The value of $k_{nr}$ increases as the emission energy decreases. Because $k_{nr}$ is much larger than $\Gamma$, the

**Table 20.1**. Spectral properties of the Rhenium MLC fac-Re(bpy)$(CO)_3$L[a]

| L | $\lambda_{em}$ (nm) | $Q$ | $\tau$ (ns) | $\Gamma$ ($s^{-1}$) | $k_{nr}$ ($s^{-1}$) |
|---|---|---|---|---|---|
| $Cl^-$ | 622 | 0.005 | 51 | $9.79 \times 10^4$ | $1.95 \times 10^7$ |
| 4-$NH_2$ Py | 597 | 0.052 | 129 | $4.06 \times 10^5$ | $7.34 \times 10^6$ |
| Py | 558 | 0.16 | 669 | $2.36 \times 10^5$ | $1.26 \times 10^6$ |
| $CH_3$ CN | 536 | 0.41 | 1201 | $3.43 \times 10^5$ | $4.90 \times 10^5$ |

[a]Data from [124].

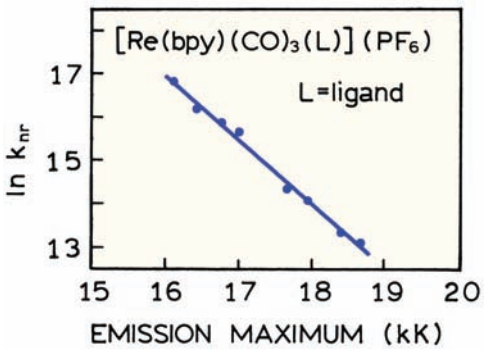


**Figure 20.29**. Dependence of the non-radiative decay rate of Re(I) complexes on the emission maxima. Revised and reprinted with permission from [124]. Copyright © 1983, American Chemical Society.

decay times of these complexes are determined mostly by the value of $k_{nr}$.

Another example of the energy gap law is shown in Figure 20.30 and Table 20.2 for osmium complexes. In this case the shortest-wavelength (highest energy) emission was found for the osmium complex with two phosphine (dppene) ligands. When the dppene ligands are replaced with phenanthroline ligands (phen) the emission maximum occurs at longer wavelengths. When this occurs the quantum yield ($Q$) and lifetime decreases in agreement with the energy gap law. These decreases are due to an increase in the non-radiative decay rate. The energy gap law is useful in understanding how the quantum yield and lifetime are related to the emission maxima, but it cannot be used to compare different types of complexes. The energy gap law works well within one homologous series of complexes, but is less useful when comparing different types of complexes.

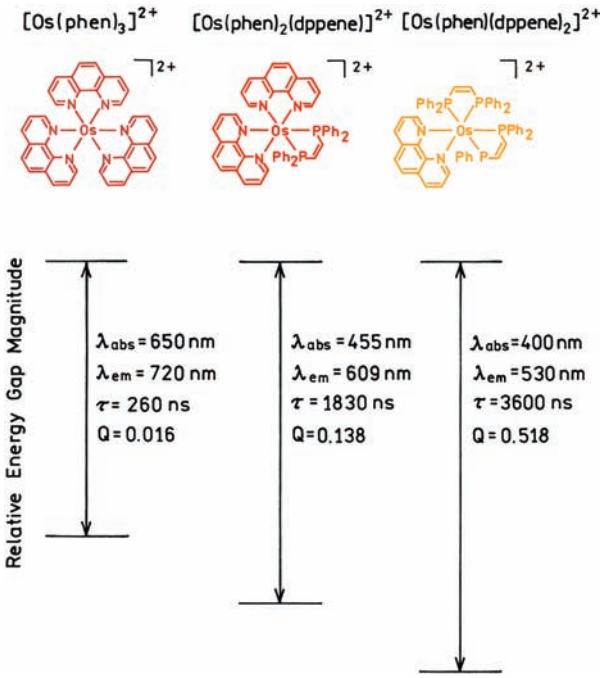


**Figure 20.30**. Osmium MLCs with different lifetimes and quantum yields. See Table 20.2.

**Table 20.2**. Spectral Properties of Osmium MLCs[a]

| Compound | $\lambda_{em}$ (nm) | $Q$ | $\tau$ (ns) | $\Gamma$ ($s^{-1}$) | $k_{nr}$ ($s^{-1}$) |
|---|---|---|---|---|---|
| $[Os(phen)_3]^{2+}$ | 720 | 0.016 | 260 | $6.15 \times 10^4$ | $3.79 \times 10^6$ |
| $[Os(phen)_2$ dppene$]^{2+}$ | 609 | 0.138 | 1830 | $7.54 \times 10^4$ | $4.71 \times 10^5$ |
| $[Os(phen)$ $(dppene)_2]^{2+}$ | 530 | 0.518 | 3600 | $1.44 \times 10^5$ | $1.37 \times 10^5$ |

[a]Data from [125].

### 20.3.5. Biophysical Applications of Metal–Ligand Probes

The MLCs can be used as biophysical probes. We present three representative applications: studies of DNA dynamics, measurement of domain–to-domain motions in proteins, and examples of metal-ligand lipid probes.

*DNA Dynamics with Metal–Ligand Probes*: Some metal–ligand complexes bind spontaneously to DNA. The strength of binding depends on the ligands and stereochemistry of the complexes. The MLCs have been used to probe DNA,[131–138] and some MLCs are quenched by nearby guanine residues.[139–141] One application is to study DNA dynamics using the polarized emission.[142–145] A spherical molecule will display a single correlation time, and, in general, globular proteins display closely spaced correlation times due to overall rotational diffusion. In contrast, DNA is highly elongated and expected to display motions on a wide range of timescales: from ns to μs (Section 12.8). Most experimental studies of DNA dynamics have been performed using ethidium bromide (EB), which displays a decay time for the DNA-bound state near 30 ns, or acridine derivatives that display shorter decay times. The short decay times of most DNA-bound dyes is a serious limitation because DNA is expected to display a wide range of relaxation times, and only the ns motions will affect the anisotropy of ns probes. In fact, most studies of DNA dynamics report only the torsional motions of DNA, which are detectable on the ns timescale. The slower bending motions of DNA are often ignored when using ns probes. These slower binding motions may be important for packaging of DNA into chromosomes.

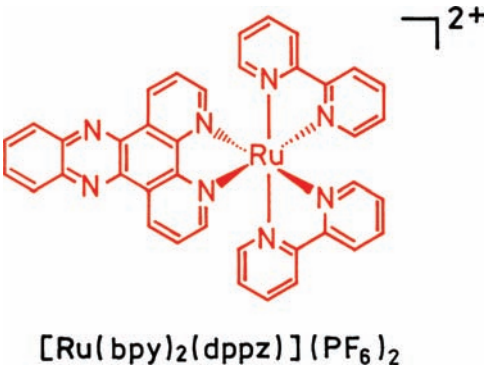


**Figure 20.31**. Chemical structure of a DNA anisotropy probe, $[Ru(bpy)_2(dppz)]^{2+}$.

An MLC probe that intercalates into double-helical DNA is shown in Figure 20.31. This probe is quenched in water and is highly luminescent when bound to DNA. The emission spectrum of $[Ru(bpy)_2(dppz)]^{2+}$ bound to calf thymus DNA is shown in Figure 20.32. In aqueous solution the probe luminescence is nearly undetectable. In the presence of DNA the luminescence of $[Ru(bpy)_2dppz]^{2+}$ is dramatically enhanced,[146–147] an effect attributed to intercalation of the dppz ligand into double-helical DNA. This MLC is highly luminescent in aprotic solvents but is dynamically quenched by water or alcohols.[148–149] The increase in fluorescence upon binding to DNA is due to shielding of the nitrogens on the dppz ligand from the solvent. This enhancement of emission upon binding to DNA means that the probe emission is observed from only the DNA-bound forms, without contributions from free probe in solution. In this respect $[Ru(bpy)_2(dppz)]^{2+}$ is analogous to ethidium bromide, which also displays significant emission from only the DNA-bound form.

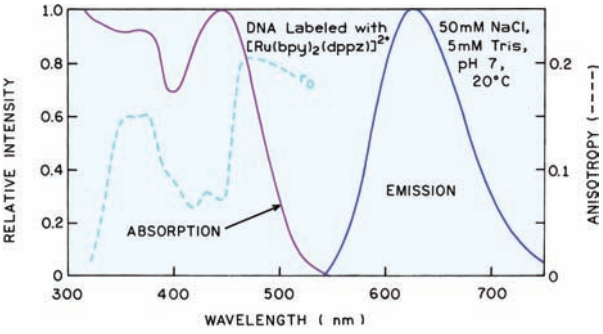


**Figure 20.32**. Absorption, emission, and excitation anisotropy spectra (dashed) of $[Ru(bpy)_2(dppz)]^{2+}$ bound to calf thymus DNA. The excitation anisotropy spectrum is in 100% glycerol at –60°C. From [144].

In order to be useful for anisotropy measurements, a probe must display a large fundamental anisotropy ($r_0$). The excitation anisotropy spectrum of $[Ru(bpy)_2(dppz)]^{2+}$ in vitrified solution (glycerol, –60°C) displays maxima at 365 and 490 nm (Figure 20.32). The high value of the anisotropy indicates that the excitation is localized on one of the organic ligands, not randomized among the ligands. It seems reasonable to conclude that the excitation is localized on the dppz ligand because shielding of the dppz ligand results in an increased quantum yield. The time-resolved intensity decay of $[Ru(bpy)_2(dppz)]^{2+}$ bound to calf thymus DNA is shown in Figure 20.33. The intensity decay is best fit by a triple-exponential decay with a mean decay time near 110 ns. Anisotropy decay can typically be measured to about three times the lifetime, suggesting that $[Ru(bpy)_2dppz]^{2+}$ can be used to study DNA dynamics to 300 ns or longer.

The time-resolved anisotropy decay of DNA-bound $[Ru(bpy)_2(dppz)]^{2+}$ is shown in Figure 20.34. The anisotropy decay could be observed to 250 ns, several-fold longer than possible with EB. The anisotropy decay appears to be a triple exponential, with apparent correlation times as long as 189.9 ns. Future intercalative MLC probes may display

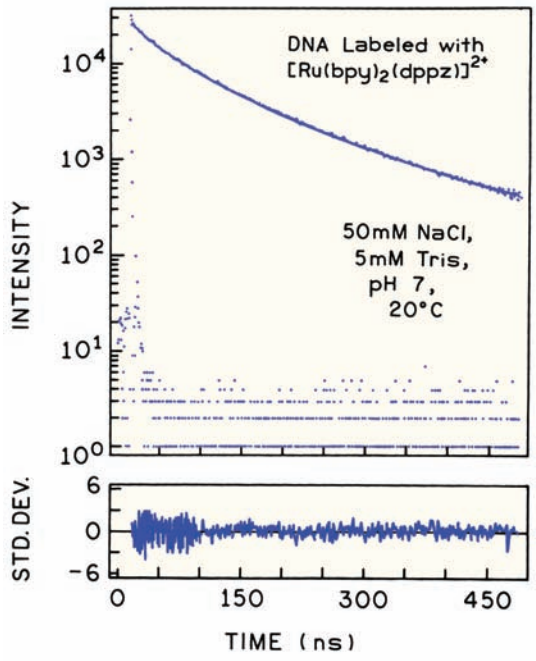


**Figure 20.33**. Time-dependent intensity decay of DNA labeled with $[Ru(bpy)_2(dppz)]^{2+}$. The data are shown as dots. The solid line and deviations (lower panel) are for the best three decay time fit, with decay times of 12.4, 46.6, and 126 ns. From [144].

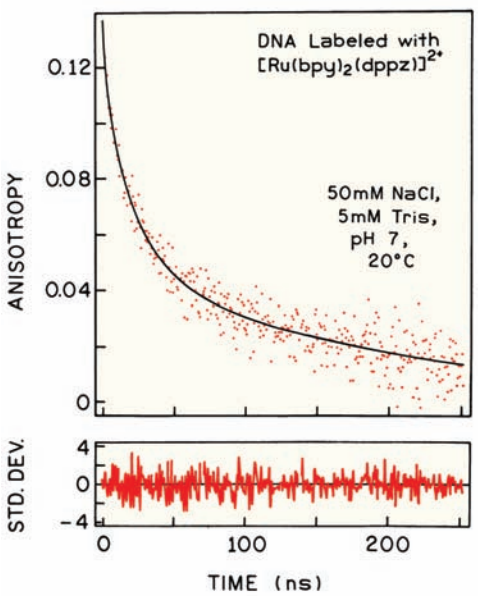


**Figure 20.34**. Time-dependent anisotropy decay of DNA labeled with $[Ru(bpy)_2(dppz)]^{2+}$. The data are shown as dots. The solid line and deviations (lower panel) are for the best three correlation time fits with correlation times of 3.1, 22.2, and 189.9 ns. From [144].

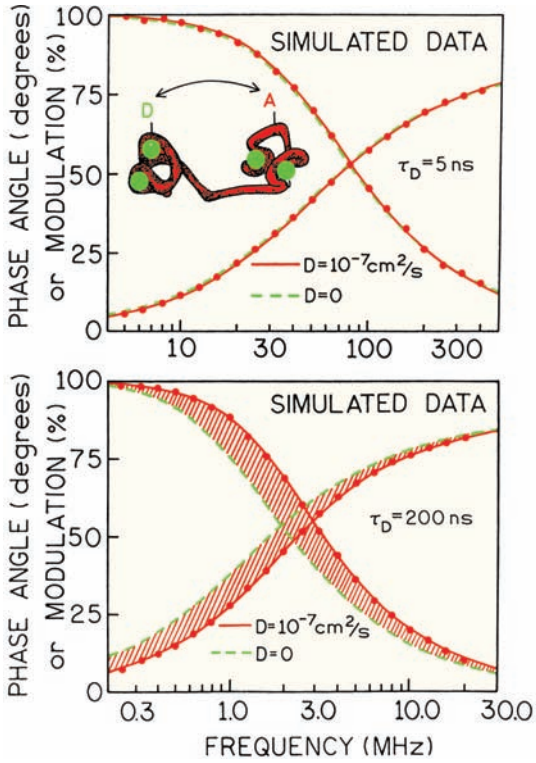


**Figure 20.35**. Simulated data illustrating effect of donor lifetime on the contribution of interdomain diffusion to the frequency-domain donor decays. For the simulations we assumed a D–A distance distribution with $R_0$ = = 30 Å and $hw$ = 20 Å. The insert shows a schematic donor (D) and acceptor (A) labeled domains for calmodulin. Top: for a donor decay time of 5 ns. Bottom: for a donor decay time of 200 ns.

longer decay times. Studies of DNA-bound MLC probes offers the opportunity to increase the information content of the time-resolved measurements of nucleic acids by extending the observations to the microsecond timescale.

*Domain-to-Domain Motions in Proteins*: There is presently considerable interest in measuring the rates of domain flexing in multi-domain proteins. Domain motions in proteins occur in signaling proteins such as calmodulin and sugar receptors. Domain motions are thought to occur in proteins such as hexokinase,[150] creatine kinase,[151–152] protein kinase C, phosphoglycerate kinase,[153] and immunoglobulin.[153–155] As described in Section 14.7, such motions can be detected by the effects of donor-to-acceptor diffusion on the extent of resonance energy transfer. These measurements have not been successful to date, primarily because the decay time of most fluorophores is too short for significant motion during the excited state lifetime.[153] This fact is illustrated in Figure 20.35, which considers the effect of D-to-A diffusion on the donor decay, as measured in the frequency domain. For domain-to-domain motions the mutual diffusion coefficients are expected to be $10^{-7}$ cm$^2$/s, or smaller. If the donor decay time is 5 ns, then diffusion has essentially no effect on the extent of energy transfer (top). For this reason the donor decay contains no information on the diffusion coefficient and cannot be used to recover the diffusion coefficient. Suppose now the donor decay time is increased to 200 ns. Then a diffusion coefficient of $10^{-7}$ cm$^2$/s has a significant effect on the extent of resonance energy transfer (RET), as shown by the shaded area in the bottom panel of Figure 20.35. To date, RET with MLCs has not been used to measure domain flexing in proteins. However, the potential seems clear, especially in light of the long decay times possible with rhenium MLCs. Decay times as long as 4 μs have been found in aqueous solution,[119] suggesting that domain flexing will be measurable with D values smaller than $10^{-8}$ cm$^2$/s.

*MLC Lipid Probes*: Long-lifetime probes are expected to be especially valuable in membrane biophysics. Long-lifetime MLC probes could be used to study rotational motions of entire lipid vesicles, or to measure diffusion by its effect on resonance energy transfer. Several MLC lipids have been described (Figure 20.36), all of which show polarized emission.[156–157] The Ru MLC lipids display life-

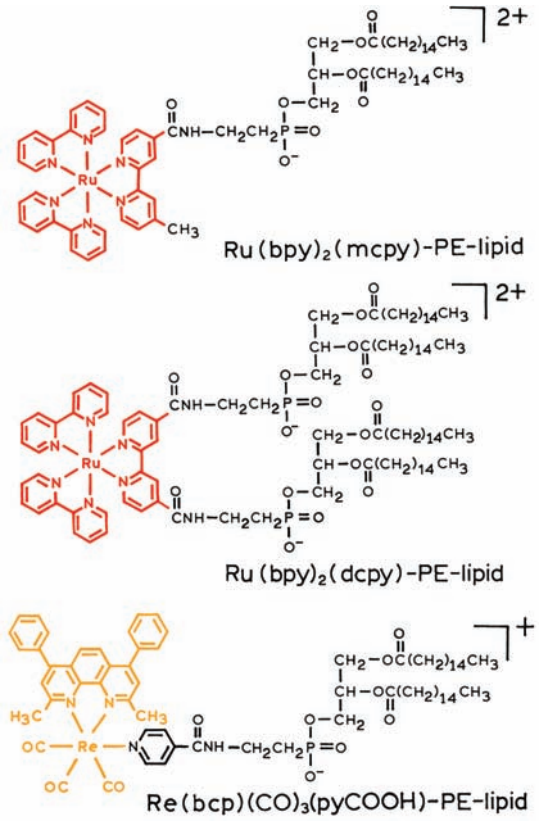


**Figure 20.36**. MLC lipid probes.

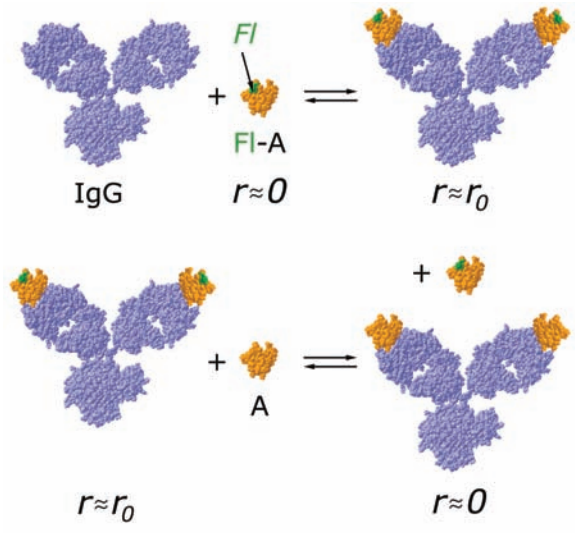


**Figure 20.37**. Schematic of a fluorescence polarization immunoassay.

times near 400 ns, and the Re MLC lipid a lifetime near 4 μs in dipalmitoyl-L-α-phosphatidylglycerol (DPPG) vesicles, in the presence of dissolved oxygen. Such long-lifetime probes can be used to measure microsecond correlation times in membranes, or even the rotational correlation times of lipid vesicles (Section 11.10.2).

### 20.3.6. MLC Immunoassays

Fluorescence-polarization immunoassays (FPIs) can be performed using MLCs.[158–162] FPIs are based on the changes in polarization (or anisotropy) that occur when a labeled drug analogue binds to an antibody specific for that drug. The anisotropy of the labeled drug can be estimated from the Perrin equation:

$$r = \frac{r_0}{1 + \tau/\Theta} \tag{20.3}$$

where $r_0$ is the anisotropy observed in the absence of rotational diffusion and $\Theta$ is the rotational correlation time. Suppose the fluorophore is fluorescein (Fl) with a lifetime near 4 ns and the analyte (A) is a small molecule with a rotational correlation time near 100 ps (Figure 20.37, top). The assay is performed using a covalent adduct of fluorescein and the analyte (Fl–A). When free in solution, the anisotropy of Fl–A is expected to be near zero. The correlation time of an antibody is near 100 ns and the anisotropy of the Fl–A–IgG complex is expected to be near $r_0$. FPIs are typically performed in a competitive format. The sample is incubated with a solution containing the labeled drug (Fl–A) and antibody (Figure 20.37, bottom). The larger the amount of unlabeled drug, the more Fl–A is displaced from the antibody, and the lower the polarization. For an FPI to be useful there needs to be a substantial difference in the anisotropy between the free and bound forms of the labeled drug.

The usefulness of MLCs in clinical FPIs is illustrated by consideration of an FPI for a higher-molecular-weight species (Figure 20.38). Suppose that the antigen is HSA, with a molecular weight near 66 kD and a rotational correlation time near 50 ns. This correlation time is already much longer than the lifetime of fluorescein, so that the anisotropy is expected to be near $r_0$. For this reason, FPIs are typically used to measure only low-molecular-weight substances.

The use of MLC probes can circumvent these limitations of FPIs to low-molecular-weight antigens. The dependence of the anisotropy on the probe lifetime and the molecular weight of the antigen is shown in Figure 20.39.

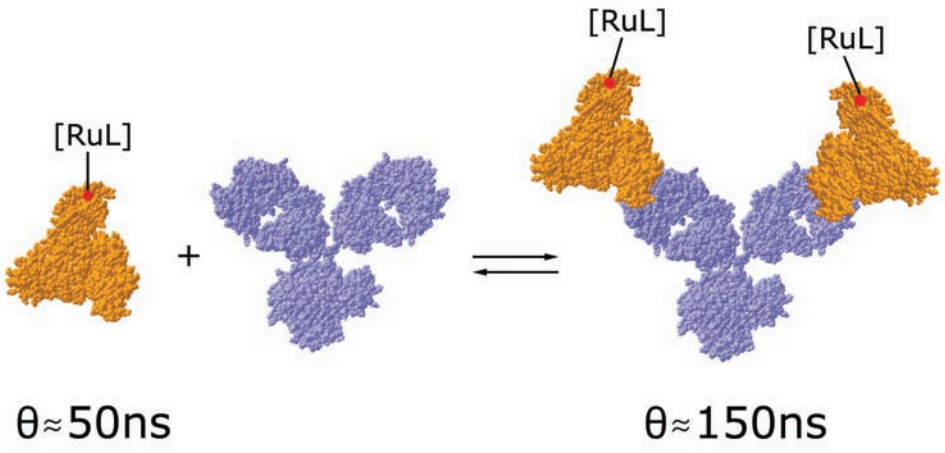


**Figure 20.38**. Fluorescence polarization immunoassay of a high-molecular-weight species using an Ru(II) metal–ligand complex.

For typical probes with lifetimes near 4 ns (fluorescein or rhodamine) the anisotropy of low-molecular-weight antigens (MW < 1000) can be estimated from Figure 20.39 to be near 0.05. An antibody has a molecular weight near 160,000, resulting in an anisotropy near 0.29 for the antigen–antibody complex. Hence a large change in anisotropy is expected upon binding of low-molecular-weight species to larger proteins or antibodies. However, if the molecular weight of the labeled antigen is larger—above 20,000 Daltons—then the anisotropy changes only slightly upon binding of the labeled antigen to a larger protein. For example, consider an association reaction that changes the molecular weight from 65,000 to 1 million daltons. Such a change could occur for an immunoassay of HSA using polyclonal antibodies, for which the effective molecular weight of the immune complexes could be 1 million or higher. In this case the anisotropy of a 4-ns probe would change from 0.278 to 0.298, which is too small of a change for quantitative purposes. In contrast, by use of a 400-ns probe, which is near the value found for our metal–ligand complex, the anisotropy value of the labeled protein with a molecular weight of 65,000 is expected to increase from 0.033 to 0.198 when the molecular weight is increased from 65,000 to 1 million daltons (Figure 20.39).

FPIs of the high-molecular-weight antigen HSA have been performed using the Ru and Re MLCs.[160–161] The Re MLC shown in Figure 20.27 displays a quantum yield of 0.2 and a lifetime over 2700 ns.[162] Absorption, emission,

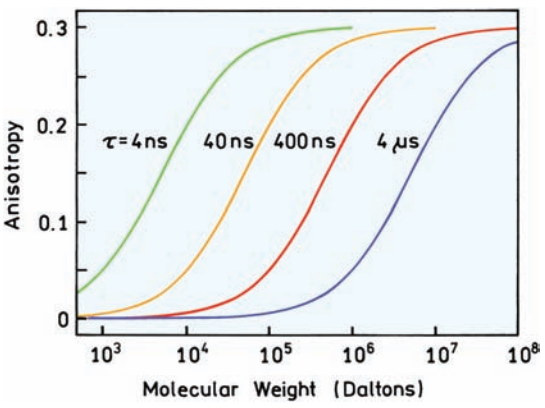


**Figure 20.39**. Molecular-weight-dependent anisotropies for probe lifetimes from 4 ns to 4 μs. The curves are based on eq. 20.3 assuming $v + h = 1.9$ ml/g for the proteins, $r_0 = 0.30$, in aqueous solution at 20°C with a viscosity of 1 cP.

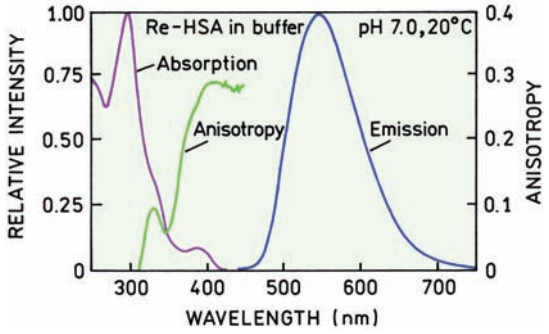


**Figure 20.40**. Absorption and emission spectra of $[Re(bcp)(CO)_3(4\text{-}COOHPy)]^+$ (RE) conjugated to HSA in 0.1 M phosphate-buffered saline (PBS) buffer, pH 7.0. Excitation wavelength was 400 nm. The excitation anisotropy spectrum in 100% glycerol at –60°C was measured with an emission wavelength of 550 nm. Reprinted with permission from [162]. Copyright © 1998, American Chemical Society.

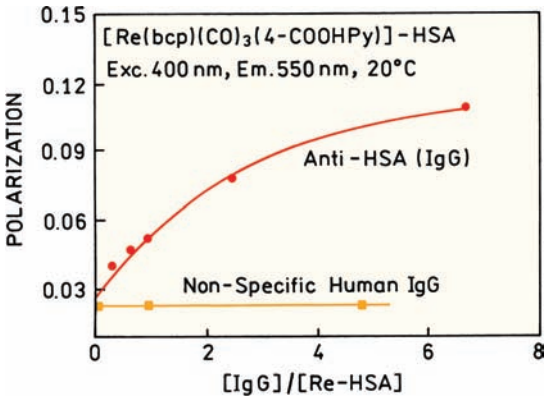


**Figure 20.41**. Steady-state fluorescence polarization of [Re(bcp)-$(CO)_3$(4-COOHPy)]–HSA at various concentrations of IgG specific for HSA (anti-HSA, circles) or nonspecific IgG (squares). Revised and reprinted with permission from [162]. Copyright © 1998, American Chemical Society.

and anisotropy spectra of this probe are shown in Figure 20.40. The Re complex can be excited near 400 nm, which is due in part to the long-wavelength absorption of the 4,7-dimethyl-1,10-phenanthroline (bcp) ligand. These wavelengths can be obtained from LEDs. The large Stokes shift from 350 to 520 nm makes it easy to isolate the MLC emission. Importantly, the Re MLC displays a high fundamental anisotropy near 0.3 for excitation at 400 nm.[162–163] This is probably due to the presence of just one chromophoric ligand, so there is no possible randomization of the excitation to other ligands.

The high-quantum-yield rhenium MLC was covalently bound to HSA used to detect binding of an antibody against human serum albumin (Figure 20.41). The steady-state anisotropy was found to increase nearly fourfold upon binding of IgG, and there was no effect from nonspecific IgG. These results demonstrated that long-lifetime MLCs are useful for immunoassays of high molecular weight antigens. It is important to note that the sensitivity of most fluorescence assays is limited not by the ability to detect the emission but rather by the presence of interfering autofluorescence that occurs on the 1- to 10-ns timescale. The availability of probes with longer decay times should also allow increased sensitivity by the use of gated detection following decay of the unwanted autofluorescence.

For many applications it is preferable to use the longest possible wavelength for excitation. At longer wavelengths there is less sample absorbance, less autofluorescence, and the light sources are less expensive. However, the quantum yields of long-wavelength MLCs are usually low. It is a challenge to obtain long-wavelength excitable MLCs that

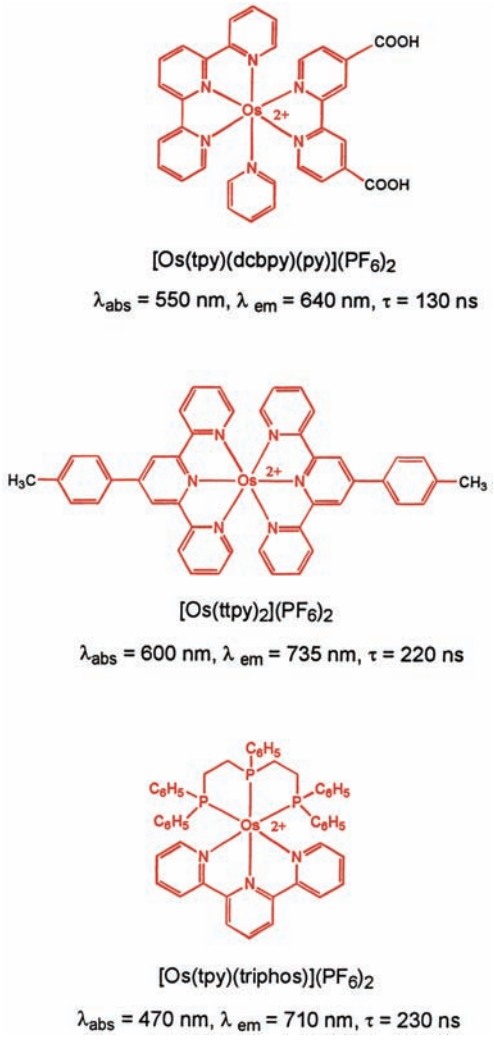


**Figure 20.42**. Long-wavelength long-lifetime osmium (II) complexes.

display long lifetimes and high quantum yields. Some progress has been made toward developing long-wavelength long-lifetime MLCs. It is known that the decay times of Os MLCs can be increased by the use of tridentate ligands in place of bidentate ligands.[164–166] Several such compounds have been synthesized (Figure 20.42). These Os complexes display long-wavelength absorption and decay times longer than 100 ns. Another approach to increasing the quantum yield and decay times of Os MLCs is by the use of arsine and phosphine ligands.[167] Using this approach it is possible to obtain high quantum yields. Unfortunately, the absorption spectra shift to shorter wavelengths, and the 450 nm absorption is weak. Some Ru MLCs display emission wavelengths as long as 715 nm and lifetimes over 100 ns.

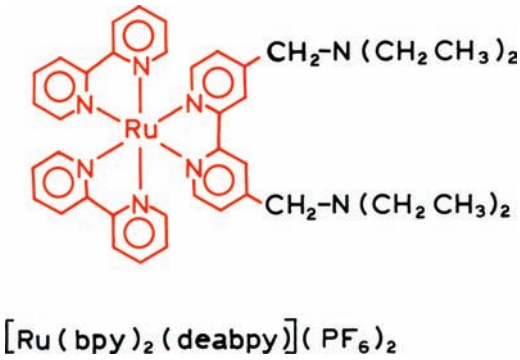


**Figure 20.43**. Structure of $[Ru(bpy)_2(deabpy)]^{2+}$, a long-lifetime MLC pH sensor. From [181].

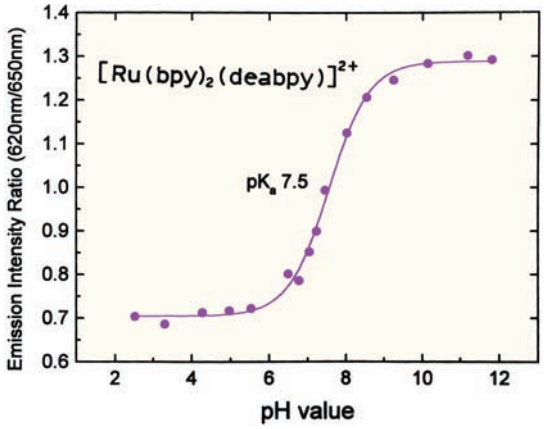


**Figure 20.45**. Wavelength-ratiometric measurements of pH using the emission intensities of $[Ru(bpy)_2(deabpy)]^{2+}$ at 620 and 650 nm. From [181].

### 20.3.7. Metal–Ligand Complex Sensors

Another area of interest is the use of MLCs in ion sensing. MLCs that are sensitive to ions[168–175] or pH[176–181] have recently become available. One example is the pH-sensitive MLC $[Ru(bpy)_2(deabpy)]^{2+}$, where deabpy is 4,4'-diethylaminomethyl-2,2'-bipyridine (Figure 20.43). The emission spectra of $[Ru(deabpy)(bpy)_2]^{2+}$ at pH values ranging from 2 to 12 are shown in Figure 20.44. The emission intensity increases about threefold as the pH increases from 2.23 to 11.75. The pH-dependent intensity changes show a $pK_A$ value near 7.5. This $pK_A$ value is ideally suited for measurements of blood pH, for which the clinically relevant range is from 7.35 to 7.46, with a central value near 7.40. In addition, much cell culture work is performed near pH 7.0–7.2. The changes in emission with a change in pH are believed to be due to deprontonation of the amino groups of $[Ru(bpy)_2(deabpy)]^{2+}$. The emission spectrum of the MLC pH probe shifts to longer wavelengths as the amino groups are prontonated at low pH (Figure 20.44). This suggests the use of $[Ru(bpy)_2(deabpy)]^{2+}$ as a wavelength-ratiometric probe (Figure 20.45). Such ratiometric probes are already in widespread use for measurement of $Ca^{2+}$ and pH (Chapter 19), but these display ns decay times.

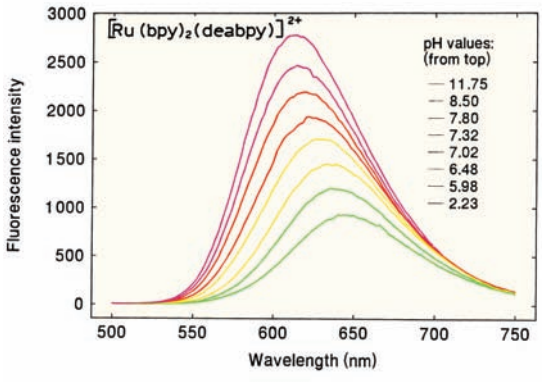


**Figure 20.44**. pH-dependent emission spectra of $Ru(bpy)_2(deabpy)(PF_6)_2$. Excitation at 414 nm. Revised from [181].

The emission shift to longer wavelengths at low pH (Figure 20.44) seems to be generally understandable in terms of the electronic properties of the excited MLCs. The long-wavelength emission is from a metal-to-ligand charge transfer (MLCT) state in which an electron is transferred from Ru to the ligand. The protonated form of deabpy is probably a better electron acceptor, lowering the energy of the MLCT state, shifting the emission to longer wavelengths, and thereby decreasing the lifetime. These results suggest a general approach to designing wavelength-ratiometric MLC probes based on cation-dependent changes in the electron affinity of the ligand. Changes in the emission spectra can be expected to cause changes in lifetime in accordance with the energy gap law (Section 20.3.4). The emission spectra (Figure 20.44) reveal that the probe is luminescent in both the protonated and unprotonated forms. This suggests that it can be useful as a lifetime probe because each form is luminescent and may display distinct decay times. At present there is an understandable interest in detection of dangerous substances. A cyanide-sensitive MLC has been reported (Figure 20.46). The emission intensity decreases as the cyanide concentration increases.

And, finally, the MLCs appear to be highly photostable. $[Ru(bpy)_2(dcbpy)]^{3+}$ and fluorescein were illuminat-

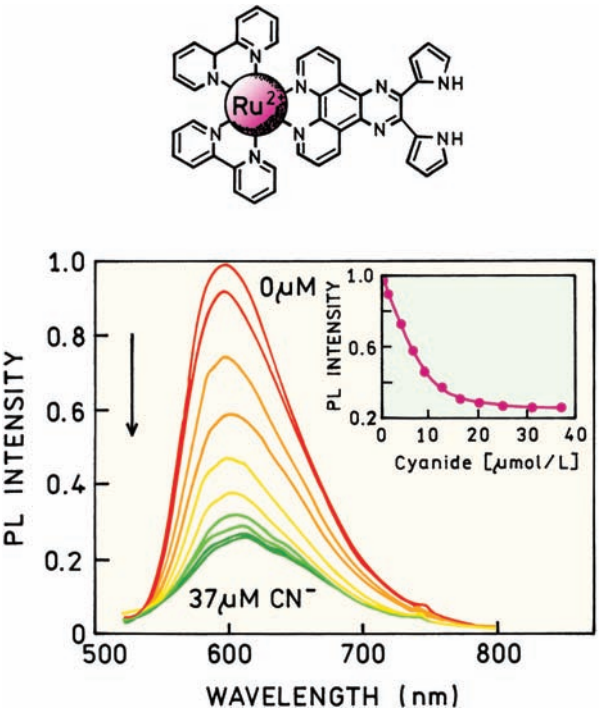


**Figure 20.46**. Structure and emission spectra of a cyanide-sensitive MLC. Revised and reprinted with permission from [175]. Copyright © 2002, American Chemical Society.

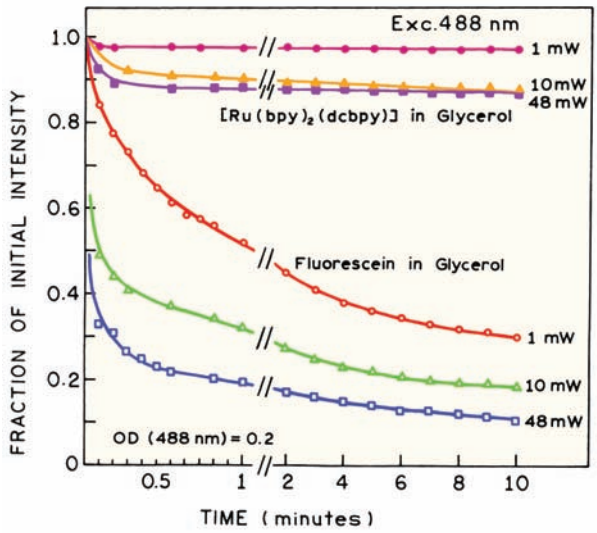


**Figure 20.47**. Photostability of $[Ru(bpy)_2(dcbpy)]^{2+}$ and fluorescein.

ed with the 488-nm output of an argon ion laser (Figure 20.47). The MLC was stable for extended periods of time, under conditions where fluorescein was rapidly bleached. The initial decrease in the MLC intensity is thought to be due to heating. The long-term photostability of MLCs should make them useful for high-sensitivity detection in fluorescence microscopy, fluorescence in-situ hybridization, and similar applications.

## 20.4. LONG-WAVELENGTH LONG-LIFETIME FLUOROPHORES

Red- and NIR-emitting probes are desirable for many applications of fluorescence. However, the red–NIR probes with high extinction coefficients and high quantum yields also display short lifetimes. For MLCs the quantum yields decrease as the emission wavelength increases, and none of the MLCs have high extinction coefficients. Some of these disadvantages of MLCs can be circumvented using MLCs as donor to high quantum-yield long-wavelength acceptors.[182–184]

A tandem MLC–red fluorophore can be used to obtain a fluorophore that has both a long emission wavelength and a long lifetime. Assume the donor is an MLC with a 1000-ns decay time and that the distance between the donor and acceptor is $r = 0.7R_0$. An acceptor at this distance will reduce the lifetime of the MLC to about 100 ns. Because the acceptor lifetime is short ($\tau_A$ = 1 ns), the acceptor intensity will closely follow the donor intensity. The acceptor will display essentially the same decay time(s) as the donor. Most acceptors will display some absorption at the donor excitation wavelength. In this case the acceptor emission will typically display an ns component as a result of a directly excited acceptor, and a long decay time near 100 ns resulting from RET from the donor. The long-lifetime emission acceptor can be readily isolated with gated detection.

An important advantage of such an RET probe is an increase in the effective quantum yield of the long-lifetime D–A pairs. This increase in quantum yield occurs because the transfer efficiency can approach unity even though the donor quantum yield is low. The result of efficient RET from the donor is that the wavelength integrated intensity of the D–A pair can be larger than that of the donor or acceptor alone (Figure 20.48). Thus tandem RET probes with MLC donors can be used to create long-lifetime probes, with red–NIR emission, with the added advantage of an increased quantum yield for the D–A pair. The modular design of these probes allows adjustment of the spectral properties, including the excitation and emission wavelengths and the decay times.

At first glance an increase in the overall quantum yield due to RET is a surprising result, but some simple consid-

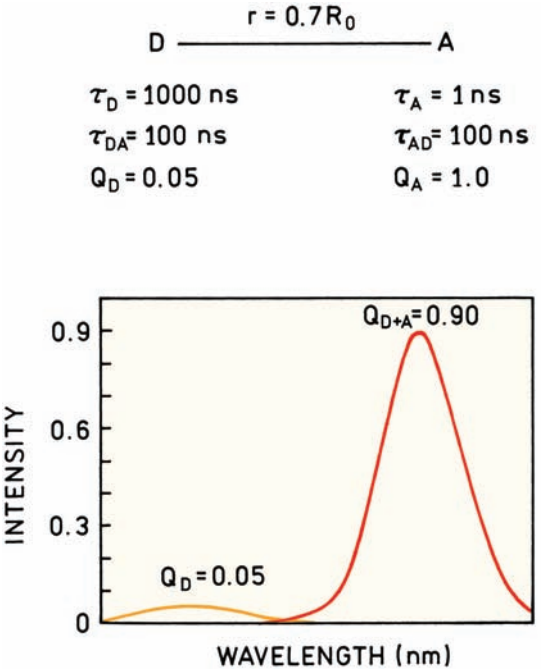


**Figure 20.48**. Schematic of a long-lifetime probe based on RET. For the simulated spectra we assumed the acceptor does not absorb at the donor excitation wavelength.

erations explain why this occurs. Consider a mixture of donor and acceptor where RET does not occur. The total emission of both the donor and acceptor is given by the sum of the two emissions. This total intensity is given by

$$F_T^0 = F_D^0 + F_A^0 = Q_D^0 \varepsilon_D + Q_A^0 \varepsilon_A \qquad (20.4)$$

where $Q_D{}^0$ and $Q_A{}^0$ are the quantum yields of the donor and acceptor in the absence of RET, and $\varepsilon_D$ and $\varepsilon_A$ are the extinction coefficients of the donor and acceptor, respectively. Now assume RET occurs with efficiency $E$. The total emission is now given by

$$F_T = F_D + F_A = Q_D^O \varepsilon_D (1 - E) + Q_A^O (\varepsilon_A + E\varepsilon_D) \qquad (20.5)$$

If the transfer efficiency is high the total intensity becomes

$$F_T = Q_A(\varepsilon_A + \varepsilon_D) \qquad (20.6)$$

so that the total quantum yield is determined by the quantum yield of the acceptor, and not the donor.

If the acceptor does not absorb at the donor excitation wavelength, then

$$F_T = Q_A \varepsilon_D \qquad (20.7)$$

so that the total quantum yield is determined by the quantum yield of the acceptor, and not the donor.

If the energy transfer is too efficient then the donor lifetime will be too short. However, it is possible to find conditions where the quantum yield is substantially increased and the acceptor lifetime is still acceptably long. An Ru MLC donor and a high-quantum-yield acceptor were linked by an polyproline linker (Figure 20.49). The acceptor emission is considerably more intense from the D–A pair than from the

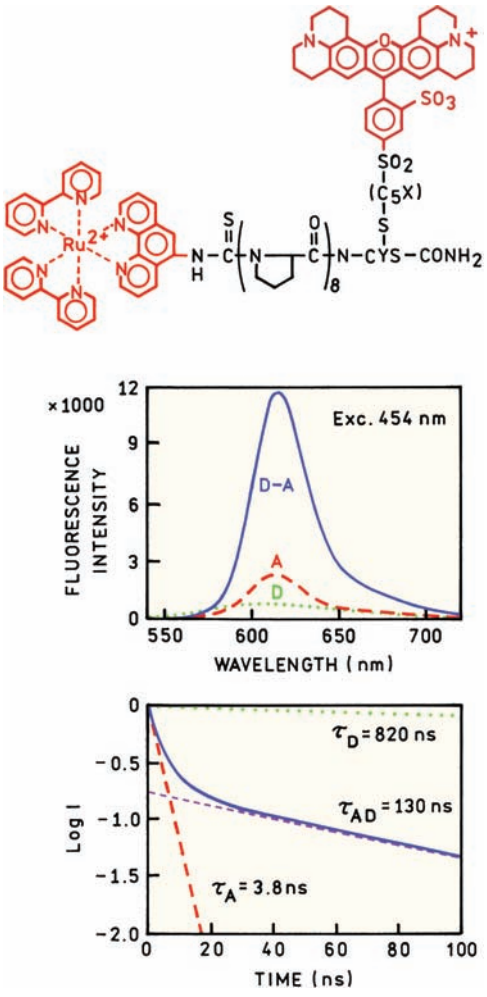


**Figure 20.49**. Structure of a tandem MLC–acceptor pair emission spectra, and intensity decays reconstructed from the frequency-domain data. Revised and reprinted with permission from [184]. Copyright © 2001, American Chemical Society.

donor or acceptor alone. In the absence of RET the donor lifetime is 820 ns. In the D–A pair the long component in the acceptor lifetime is 130 ns, which is long enough to use with gated detection. These results show a general approach to obtain the desired emission wavelengths and lifetime using MLCs as donors in tandem probes.

## REFERENCES


1. Bruchez M, Moronne M, Gin P, Weiss S, Alivisatos AP. 1998. Semiconductor nanocrystals as fluorescent biological labels. *Science* **281**: 2013–2016.
2. Watson A, Wu X, Bruchez M. 2003. Lighting up cells with quantum dots. *Biotechnology* **34**:296–303.
3. Pietryga JM, Schaller RD, Werder D, Stewart MH, Klimov VI, Hollingsworth JA. 2004. Pushing the band gap envelope: mid-infrared emitting colloidal PbSe quantum dots. *J Am Chem Soc* **126**: 11752–11753.
4. Kuczynski JP, Milosavljevic BH, Thomas JK. 1983. Effect of the synthetic preparation on the photochemical behavior of colloidal CdS. *J Phys Chem* **87**:3368–3370.
5. Rossetti R, Nakahara S, Brus LE. 1983. Quantum size effects in the redox potentials, resonance Raman spectra, and electronic spectra of CdS crystallites in aqueous solution. *J Chem Phys* **79**(2):1086–1088.
6. Weller H, Koch U, Gutierrez M, Henglein A. 1984. Photochemistry of colloidal metal sulfides: absorption and fluorescence of extremely small ZnS particles (the world of the neglected dimensions). *Ber Bunsenges Phys Chem* **88**:649–656.
7. Ramsden JJ, Gratzel M. 1984. Photoluminescence of small cadmium sulphide particles. *J Chem Soc Faraday Trans* **80**:919–933.
8. Murray CB, Kagan CR, Bawendi MG. 2000. Synthesis and characterization of monodisperse nanocrystals and close-packed nanocrystal assemblies. *Annu Rev Mater Sci* **30**:545–610.
9. Gerion D, Pinaud F, Williams SC, Parak WJ, Zanchet D, Weiss S, Alivisatos AP. 2001. Synthesis and properties of biocompatible water-soluble silica-coated CdSe/ZnS semiconductor quantum dots. *J Phys Chem B* **105**:8861–8871.
10. Kortan AR, Hull R, Opila RL, Bawendi MG, Steigerwald ML, Carroll PJ, Brus LE. 1990. Nucleation and growth of CdSe on ZnS quantum crystallite seeds, and vice versa, in inverse micelle media. *J Am Chem Soc* **112**:1327–1332.
11. Dabbousi BO, Rodriquez-Viejo J, Mikulec FV, Heine JR, Mattoussi H, Ober R, Jensen KF, Bawendi MG. 1997. (CdSe)ZnS core-shell quantum dots: synthesis and characterization of a size series of highly luminescent nanocrystallites. *J Phys Chem B* **101**:9463–9475.
12. Alivisatos AP. 1996. Perspectives on the physical chemistry of semiconductor nanocrystals. *J Phys Chem* **100**:13226–13239.
13. Murphy CJ, Coffer JL. 2002. Quantum dots: a primer. *Appl Spectrosc* **56**:16A–27A.
14. Parak WJ, Gerion D, Pellegrino T, Zanchet D, Micheel C, Williams SC, Boudreau R, Le Gros MA, Larabell CA, Alivisatos AP. 2003. Biological applications of colloidal nanocrystals. *Nanotechnology* **14**:R15–R27.
15. Bawendi MG, Steigerwald ML, Brus LE. 1990. The quantum mechanics of larger semiconductor clusters ("quantum dots"). *Annu Rev Phys Chem* **41**:477–496.
16. Weller H. 1993. Colloidal semiconductor Q-particles: chemistry in the transition region between solid state and molecules. *Angew Chem, Int Ed* **32**(1):41–53.
17. Goldman ER, Anderson GP, Tran PT, Mattoussi H, Charles PT, Mauro JM. 2002. Conjugation of luminescent quantum dots with antibodies using an engineered adaptor protein to provide new reagents for fluoroimmunoassays. *Anal Chem* **74**:841–847.
18. Goldman ER, Balighian ED, Mattoussi H, Kuno MK, Mauro JM, Tran PT, Anderson GP. 2002. Avidin: a natural bridge for quantum dot-antibody conjugates. *J Am Chem Soc* **124**:6378–6382.
19. Jovin TM. 2003. Quantum dots finally come of age. *Nature Biotechnol* **21**:32–33.
20. Chan WCW, Maxwell DJ, Gao X, Bailey RE, Han M, Nie S. 2002. Luminescent quantum dots for multiplexed biological detection and imaging. *Curr Opin Biotechnol* **13**:40–46.
21. Jares-Erijman E, Jovin TM. 2003. FRET imaging. *Nature Biotechnol* **21**(11):1387–1395.
22. Gerion D, Chen F, Kannan B, Fu A, Parak WJ, Chen DJ, Majumdar A, Alivisatos AP. 2003. Room-temperature single-nucleotide polymorphism and multiallele DNA detection using fluorescent nanocrystals and microarrays. *Anal Chem* **75**:4766–4772.
23. Goldman ER, Clapp AR, Anderson GP, Uyeda HT, Mauro JM, Medintz IL, Mattoussi H. 2004. Multiplexed toxin analysis using four colors of quantum dot fluororeagents. *Anal Chem* **76**:684–688.
24. Gao X, Chan WCW, Nie S. 2002. Quantum-dot nanocrystals for ultrasensitive biological labeling and multicolor optical encoding. *J Biomed Optics* **7**(4):532–537.
25. Leatherdale CA, Woo WK, Mikulec FV, Bawendi MG. 2002. On the absorption cross-section of CdSe nanocrystal quantum dots. *J Phys Chem B* **106**:7619–7622.
26. Schmelz O, Mews A, Basche T, Herrmann A, Mullen K. 2001. Supramolecular complexes from CdSe nanocrystals and organic fluorophors. *Langmuir* **17**:2861–2865.
27. Derfus AM, Chan WCW, Bhatia SN. 2004. Probing the cytotoxicity of semiconductor quantum dots. *Nanotechnol Lett* **4**(1):11–18.
28. Hoshino A, Fujioka K, Oku T, Suga M, Sasaki YF, Ohta T, Yasuhara M, Suzuki K, Yamamoto K. 2004. Physicochemical properties and cellular toxicity of nanocrystal quantum dots depend on their surface modification. *Nanotechnol Lett* **4**(11):2163–2169.
29. Dubertret B, Skourides P, Norris DJ, Noireaux V, Brivanlou AH, Libchaber A. 2002. In vivo imaging of quantum dots encapsulated in phospholipid micelles. *Science* **298**(5599):1759–1762.
30. Wu X, Liu H, Liu J, Haley KN, Treadway JA, Larson JP, Ge N, Peale F, Bruchez M. 2003. Immunofluorescent labeling of cancer marker Her2 and other cellular targets with semiconductor quantum dots. *Nature Biotechnol* **21**:41–46.
31. Jaiswal JK, Mattoussi H, Mauro JM, Simon SM. 2003. Long-term multiple color imaging of live cells using quantum dot bioconjugates. *Nature Biotechnol* **21**:47–51.
32. Wargnier R, Baranov AV, Maslov VG, Stsiapura V, Artemyev M, Pluot M, Sukhanova A, Nabiev I. 2004. Energy transfer in aqueous solutions of oppositely charged CdSe/ZnS core-shell quantum dots and in quantum dot-nanogold assemblies. *Nanotechnol Lett* **4**(3): 451–457.

33. Achermann M, Petruska MA, Crooker SA, Klimov VI. 2003. Picosecond energy transfer in quantum dot Langmuir-Blodgett nanoassemblies. *J Phys Chem B* **107**:13782–13787.
34. Kagan CR, Murray CB, Nirmal M, Bawendi MG. 1996. Electronic energy transfer in CdSe quantum dot solids. *Phys Rev Lett* **76**(9): 1517–1520.
35. Kagan CR, Murray CB, Bawendi MG. 1996. Long-range resonance transfer of electronic excitations in close-packed CdSe quantum-dot solids. *Phys Rev B* **54**(12):8633–8643.
36. Mamedova NN, Kotov NA, Rogach AL, Studer J. 2001. Albumin-CdTe nanoparticle bioconugates: preparation, structure, and interunit energy transfer with antenna effect. *Nanotechnol Lett* **1**(6):281–286.
37. Javier A, Yun CS, Sorena J, Strouse GF. 2003. Energy transfer in CdSe nanocrystals assembled with molecular wires. *J Phys Chem B* **107**:435–442.
38. Kloepfer JA, Cohen N, Nadeau JL. 2004. FRET between CdSe quantum dots in lipid vesicles and water- and lipid-soluble dyes. *J Phys Chem B* **108**:17042–17049.
39. Willard DM, Carillo LL, Jung J, Van Orden A. 2001. CdSe-ZnS quantum dots as resonance energy transfer donors in a model protein–protein binding assay. *Nanotechnol Lett* **1**(9):469–474.
40. Martin RB, Richardson FS. 1979. Lanthanides as probes for calcium in biological systems. *Q Rev Biophys* **12**(2):181–209.
41. Horrocks WD, Albin M. 1984. Lanthanide ion luminescence in coordination chemistry and biochemistry. *Prog Inorg Chem* **31**:1–104.
42. Turro C, Fu PKL, Bradley PM. 2003. Lanthanide ions and luminescent probes of proteins and nucleic acids. In *The lanthanides and their interrelations with biosystems*, pp. 323–353. Ed A Sigel, H Sigel. Marcel Dekker, New York.
43. Lis S. 1992. Luminescence lifetime measurements of lanthanide aquo ions and their complexes: hydration study of Eu(III) systems. *Mater Sci.* **18**(2–4):51–60.
44. Choppin GR, Peterman DR. 1998. Applications of lanthanide luminescence spectroscopy to solution studies of coordination chemistry. *Coord Chem Rev* **174**:283–299.
45. Sabbatini N, Guardigli M, Manet I. 1997. Lanthanide complexes of encapsulating ligands as luminescent devices. In *Advances in photochemistry*, Vol. 23, pp. 213–278. Ed DC Neckers, DH Volman, G von Bünau. John Wiley & Sons, New York.
46. Selvin PR. 1999. Luminescent lanthanide chelates for improved resonance energy transfer and application to biology. In *Applied fluorescence in chemistry, biology and medicine*, pp. 457–487. Ed W Rettig, B Strehmel, S Schrader, H Seifert. Springer, New York.
47. de Sa GF, Malta OL, de Mello Donega C, Simas AM, Longo RL, Santa-Cruz PA, de Silva EF. 2000. Spectroscopic properties and design of highly luminescent lanthanide coordination complexes. *Coord Chem Rev* **196**:165–195.
48. Bakker BH, Goes M, Hoebe N, van Ramesdonk HJ, Verhoeven JW, Werts MHV, Hofstraat JW. 2000. Luminescent materials and devices: lanthanide azatriphenylene complexes and electroluminescent charge transfer systems. *Coord Chem Rev* **208**:3–16.
49. Heyduk E, Heyduk T. 1997. Thiol-reactive, luminescent europium chelates: luminescence probes for resonance energy transfer distance measurements in biomolecules. *Anal Biochem* **248**:216–227.
50. Ge P, Selvin PR. 2003. Thiol-reactive luminescent lanthanide chelates, part 2. *Bioconjugate Chem* **14**:870–876.
51. Yuan J, Wang G, Majima K, Matsumoto K. 2001. Synthesis of a terbium fluorescent chelate and its application to time-resolved fluoroimmunoassay. *Anal Chem* **73**:1869–1876.
52. Roy BC, Santos M, Mallik S, Campiglia AD. 2003. Synthesis of metal-chelating lipids to sensitive lanthanide ions. *J Org Chem* **68**: 3999–4007.
53. Wu FB, Zhang C. 2002. A new europium β-diketone chelate for ultrasensitive time-resolved fluorescence immunoassays. *Anal Biochem* **311**:57–67.
54. Hemmila I, Mukkala VM, Takalo H. 1997. Development of luminescent lanthanide chelate labels for diagnostic assays. *J Alloys Compd* **249**:158–162.
55. Selvin PR, Hearst JE. 1994. Luminescence energy transfer using a terbium chelate: improvements on fluorescence energy transfer. *Proc Natl Acad Sci USA* **91**:10024–10028.
56. Chen J, Selvin PR. 2000. Lifetime- and color-tailored fluorophores in the micro- to millisecond time regime. *J Am Chem Soc* **122**: 657–660.
57. Selvin PR, Rana TM, Hearst JE. 1994. Luminescence resonance energy transfer. *J Am Chem Soc* **116**:6029–6030.
58. Sueda S, Yuan J, Matsumoto K. 2002. A homogeneous DNA hybridization system by using a new luminescence terbium chelate. *Bioconjugate Chem* **13**:200–205.
59. Okabayashi Y, Ikeuchi I. 1998. Liposome immunoassay by long-lived fluorescence detection. *Analyst* **123**:1329–1332.
60. Chen Y, Lehrer SS. 2004. Distances between tropomyosin sites across the muscle thin filament using luminescence resonance energy transfer: evidence for tropomyosin flexibility. *Biochemistry* **43**: 11491–11499.
61. Kessler MA. 1999. Probing the dissociation state of acid-base indicators by time-resolved lanthanide luminescence: a convenient transduction scheme for optical chemical sensors. *Anal Chem* **71**: 1540–1543.
62. Gunnlaugsson T, Mac Donaill D, Parker D. 2001. Lanthanide macrocyclic quinolyl conjugates as luminescent molecular-level devices. *J Am Chem Soc* **123**:12866–12876.
63. Lowe MP, Parker D, Reany O, Aime S, Botta M, Castellano G, Gianolio E, Pagliarin R. 2001. pH-dependent modulation of relaxivity and luminescence in macrocyclic gadolinium and europium complexes based on reversible intramolecular sulfonamide ligation. *J Am Chem Soc* **123**:7601–7609.
64. Hanaoka K, Kikuchi K, Kojima H, Urano Y, Nagano T. 2004. Development of a zinc ion-selective luminescent lanthanide chemosensor for biological applications. *J Am Chem Soc* **126**: 12470–12476.
65. Blair S, Lowe MP, Mathieu CE, Parker D, Senanayake PK, Kataky R. 2001. Narrow-range optical pH sensors based on luminescent europium and terbium complexes immobilized in a sol gel glass. *Inorg Chem* **40**:5860–5867.
66. Lowe MP, Parker D. 2000. Controllable pH modulation of lanthanide luminescence by intramolecular switching of the hydration state. *Chem Commun* **8**:707–708.
67. Mortellaro MA, Nocera DG. 1996. A supramolecular chemosensor for aromatic hydrocarbons. *J Am Chem Soc* **118**:7414–7415.
68. Harma H, Soukka T, Lovgren T. 2001. Europium nanoparticles and time-resolved fluorescence for ultrasensitive detection of prostate-specific antigen. *Clin Chem* **47**(3):561–568.

69. Soukka T, Paukkunen J, Harma H, Lonnberg S, Lindroos H, Lovgren T. 2001. Supersensitive time-resolved immunofluorometric assay of free prostate-specific antigen with nanoparticle label technology. *Clin Chem* **47**(7):1269–1278.
70. Riwotzki K, Meyssamy H, Kornowski A, Haase M. 2000. Liquid-phase synthesis of doped nanoparticles: colloids of luminescing $LaPO_4$:Eu and $CePO_4$:Tb particles with a narrow particle size distribution. *J Phys Chem B* **104**:2824–2828.
71. Ye Z, Tan M, Wang G, Yuan J. 2004. Preparation, characterization, and time-resolved fluorometric application of silica-coated terbium (III) fluorescence nanoparticles. *Anal Chem* **76**:513–518.
72. Werts MHV, Hofstraat JW, Geurts FAJ, Verhoeven JW. 1997. Fluorescein and eosin as sensitizing chromophores in near-infrared luminescent ytterbium (III), neodymium (III) and erbium (III) chelates. *Chem Phys Lett* **276**:196–201.
73. Hebbink GA, Grave L, Woldering LA, Reinhoudt DN, van Veggel FCJM. 2003. Unexpected sensitization efficiency of the near-infrared $Nd^{3+}$, $Er^{3+}$, and $Yb^{3+}$ emission by fluorescein compared to eosin and erythrosin. *J Phys Chem A* **107**:2483–2491.
74. Werts MHV, Verhoeven JW, Hofstraat JW. 2000. Efficient visible light sensitisation of water-soluble near-infrared luminescent lanthanide complexes. *J Chem Soc Perkin Trans* **2**:433–439.
75. Wang H, Qian G, Wang M, Zhang J, Luo Y. (2004). Enhanced luminescence of an eribium (III) ion-association ternary complex with a near-infrared dye. *J Phys Chem B* **108**:8084–8088.
76. Hebbink G. A. Reinhoudt, DN, van Veggel FCJM. 2001. Increased luminescent lifetimes of $Ln^{3+}$ complexes emitting in the near-infrared as a result of deuteration. *Eur J Org Chem* 4101–4106.
77. Hasegawa Y, Kimura Y, Murakoshi K, Wada Y, Kim JH, Nakashima N, Yamanaka T, Yanagida S. 1996. Enhanced emission of deuterated tris(hexafluoroacetylacetonato) neodymium (III) complex in solution by suppression of radiationless transition via vibrational excitation. *J Phys Chem* **100**:10201–10205.
78. Werts MHV, Woudenberg RH, Emmerink PG, van Gassel R, Hofstraat JW, Verhoeven JW. 2000. A near-infrared luminescent label based on $Yb^{III}$ ions and its application in a fluoroimmunoassay. *Angew Chem, Int Ed* **39**(24):4542–4544.
79. Gardner SJ, Hewlett DF. 2003. Optimization and initial evaluation of 1,2-indandione as a reagent for fingerprint detection. *J Forensic Sci* **48**(6):1–5.
80. Almog J, Cohen Y, Azoury M, Hahn TR. 2004. Genipin—a novel fingerprint reagent with colorimetric and fluorogenic activity. *J Forensic Sci* **49**(2):255–257.
81. Caldwell JP, Henderson W, Kim ND. 2001. Luminescent visualization of latent fingerprints by direct reaction with a lanthanide shift reagent. *J Forensic Sci* **46**(6):1332–1341.
82. Allred CE, Menzel ER. 1997. A novel europium-bioconjugate method for latent fingerprint detection. *Forensic Sci Int* **85**:83–94.
83. Wilkinson D. 1999. A one-step fluorescent detection method for lipid fingerprints; $Eu(TTA)_3$ 2TOPO. *Forensic Sci Int* **99**:5–23.
84. Vanderkooi JM. 1992. Tryptophan phosphorescence from proteins at room temperature. In *Topics in fluorescence spectroscopy*, Vol. 3: *Biochemical applications*, pp. 113–136. Ed JR Lakowicz. Plenum Press, New York.
85. Barthold M, Barrantes FJ, Jovin TM. 1981. Rotational molecular dynamics of the membrane-bound acetylcholine receptor revealed by phosphorescence spectroscopy. *Eur J Biochem* **120**:389–397.
86. Che A, Cherry RJ. 1995. Loss of rotational mobility of band 3 proteins in human erythrocyte membranes induced by antibodies to glycophorin A. *Biophys J* **68**:1881–1887.
87. Haugen GR, Lytle FE. 1981. Quantitation of fluorophores in solution by pulsed laser excitation and time-filtered detection. *Anal Chem* **53**:1554–1559.
88. Brewer KJ. 1999. Tridentate-bridged polyazine complexes of ruthenium (III) and osmium (III) and their application to the development of photochemical molecular devices. *Comments Inorg Chem* **21**(4–6):201–224.
89. Chen P, Meyer TJ. 1998. Medium effects on charge transfer in metal complexes. *Chem Rev* **98**:1439–1477.
90. Stufkens DJ, Vlèek Jr A. 1998. Ligand-dependent excited state behaviour of Re(I) and Ru(II) carbonyl–diimine complexes. *Coord Chem Rev* **177**:127–179.
91. Shan B-Z, Zhao Q, Goswami N, Eichhorn DM, Rillema DP. 2001. Structure, NMR and other physical and photophysical properties of ruthenium (II) complexes containing the 3,3'-dicarboxyl-2,2'-bipyridine ligand. *Coord Chem Rev* **211**:117–144.
92. Balzani V, Juris A. 2001. Photochemistry and photophysics of Ru(II)-polypyridine complexes in the bologna group: from early studies to recent developments. *Coord Chem Rev* **211**:97–115.
93. Sun S-S, Lees AJ. 2002. Transition metal based supramolecular systems: synthesis, photophysics, photochemistry and their potential applications as luminescent anion chemosensors. *Coord Chem Rev* **230**:171–192.
94. Balzani V, Sabbatini N. 1986. "Second-sphere" photochemistry and photophysics of coordination compounds. *Chem Rev* **86**:319–337.
95. Chen P, Meyer TJ. 1998. Medium effects on charge transfer in metal complexes. *Chem Rev* **98**:1439–1477.
96. Juris A, Balzani V, Barigelletti F, Campagna S, Belser P, Von Zelewsky A. 1988. Ru(II) polypyridine complexes: photophysics, photochemistry, electrochemistry and chemiluminescence. *Coord Chem Rev* **84**:85–277.
97. Demas JN, DeGraff BA. 1994. Design and applications of highly luminescent transition metal complexes. In *Topics in fluorescence spectroscopy*, Vol. 4: *Probe design and chemical sensing*, pp. 71–107. Ed JR Lakowicz. Plenum Press, New York.
98. Castellano FN. Personal communication.
99. McCusker JK. 2003. Femtosecond absorption spectroscopy of transition metal charge-transfer complexes. *Acc Chem Res* **36**:876–887.
100. Yeh AT, Shank CV, McCusker JK. 2000. Ultrafast electron localization dynamics following photo-induced charge transfer. *Science* **289**: 935–938.
101. Bhasikuttan AC, Suzuki M, Nakashima S, Okada T. 2002. Ultrafast fluorescence detection in tris(2,2'-bipyridine)ruthenium(II) complex in solution: relaxation dynamics involving higher excited states. *J Am Chem Soc* **124**:8398–8405.
102. Damrauer NH, Cerullo G, Yeh A, Boussie TR, Sharnk CV, McCusker JK. 1997. Femtosecond dynamics of excited state evolution in $[Ru(bpy)_3]^{2+}$. *Science* **275**:54–57.

103. Demas JN, DeGraff BA. 1991. Design and applications of highly luminescent transition metal complexes. *Anal Chem* **63**:829A–837A.
104. Kalayanasundaram K. 1992. *Photochemistry of polypyridine and porphyrin complexes*. Academic Press, New York.
105. Terpetschnig E, Szmacinski H, Malak. H, Lakowicz JR. 1995. Metal–ligand complexes as a new class of long-lived fluorophores for protein hydrodynamics. *Biophys J* **68**:342–350.
106. Kise KJ, Bowler BE. 2002. A ruthenium (II) tris(bipyridyl) amino acid: synthesis and direct incorporation into an α-helical peptide by solid-phase synthesis. *Inorg Chem* **41**(2):379–386.
107. Lo KK-W, Hui W-K, Ng DC-M, Cheung K-K. 2002. Synthesis, characterization, photophysical properties, and biological labeling studies of a series of luminescent rhenium (I) polypyridine maleimide complexes. *Inorg Chem* **41**(1):40–46.
108. Muheim A, Todd RJ, Casimiro DR, Gray HB, Arnold FH. 1993. Ruthenium-mediated protein cross-linking and stabilization. *J Am Chem Soc* **115**:5312–5313.
109. Rau HK, DeJonge N, Haehnel W. 1998. Modular synthesis of *de novo*-designed metalloproteins for light-induced electron transfer. *Proc Natl Acad Sci USA* **95**:11526–11531.
110. Szmacinski H, Terpetschnig E, Lakowicz JR. 1996. Synthesis and evaluation of Ru-complexes as anisotropy probes for protein hydrodynamics and immunoassays of high-molecular-weight antigens. *Biophys Chem* **62**:109–120.
111. Castellano FN, Dattelbaum JD, Lakowicz JR. 1998. Long-lifetime Ru(II) complexes as labeling reagents for sulfhydryl groups. *Anal Biochem* **255**:165–170.
112. Terpetschnig E, Dattelbaum JD, Szmacinski H, Lakowicz JR. 1997. Synthesis and spectral characterization of a thiol-reactive long-lifetime Ru(II) complex. *Anal Biochem* **251**:241–245.
113. Slim M, Sleiman HF. 2004. Ruthenium(II)–phenanthroline–biotin complexes: synthesis and luminescence enhancement upon binding to avidin. *Bioconjugate Chem* **15**(5):949–953.
114. Hu X, Smith GD, Sykora M, Lee SJ, Grinstaff MW. 2000. Automated solid-phase synthesis and photophysical properties of oligodeoxynucleotides labeled at 5'-aminothymidine with $Ru(bpy)_2$-(4-m-4'-cam-bpy)$^{2+}$. *Inorg Chem* **39**:2500–2504.
115. Khan SI, Beilstein AE, Tierney MT, Sykora M, Grinstaff MW. 1999. Solid-phase synthesis and photophysical properties of DNA labeled at the nucleobase with $Ru(bpy)_2$(4-m-4'-pa-bpy)$^{2+}$. *Inorg Chem* **38**:5999–6002.
116. Khan SI, Beilstein AE, Smith GD, Sykora M, Grinstaff MW. 1999. Synthesis and excited-state properties of a novel ruthenium nucleoside: 5[$Ru(bpy)_2$(4-m-4'-pa-bpy)]$^{2+}$-2'-deoxyuridine. *Inorg Chem* **38**: 2411–2415.
117. Khan SI, Beilstein AE, Grinstaff MW. 1999. Automated solid-phase synthesis of site-specifically labeled ruthenium-oligonucleotides. *Inorg Chem* **38**:418–419.
118. Hurley DJ, Tor Y. 1998. Metal-containing oligonucleotides: solid-phase synthesis and luminescence properties. *J Am Chem Soc* **120**:2194–2195.
119. Guo X, Li L, Castellano FN, Szmacinski H, Lakowicz JR. 1997. A long-lived, highly luminescent rhenium (I) metal–ligand complex as a bimolecular probe. *Anal Biochem* **254**:179–186.
120. Terpetschnig E, Szmacinski H, Lakowicz JR. 1996. Fluorescence polarization immunoassay of a high molecular weight antigen using a long wavelength absorbing and laser diode-excitable metal–ligand complex. *Anal Biochem* **240**:54–59.
121. Lakowicz JR, Terpetschnig E, Murtaza Z, Szmacinski H. 1997. Development of long-lifetime metal–ligand probes for biophysics and cellular imaging. *J Fluoresc* **7**(1):17–25.
122. Demas JN, DeGraff BA. 1992. Applications of highly luminescent transition metal complexes in polymer systems. *Macromol Chem, Macromol Symp* **59**:35–51.
123. Demas JN, DeGraff BA. 1997. Applications of luminescent transition metal complexes to sensor technology and molecular probes. *J Chem Educ* **74**(6):690–695.
124. Caspar J, Meyer TJ. 1983. Application of the energy gap law to nonradiative, excited-state decay. *J Phys Chem* **87**:952–957.
125. Kober EM, Marshall JL, Dressick WJ, Sullivan BP, Caspar JV, Meyer TJ. 1985. Synthetic control of excited states: nonchromophoric ligand variations in polypyridyl complexes of osmium (II). *Inorg Chem* **24**:2755–2763.
126. Kober EM, Sullivan BP, Dressick WJ, Caspar JV, Meyer TJ. 1980. Highly luminescent polypyridyl complexes of osmium (II). *J Am Chem Soc* **102**:1383–1385.
127. Caspar JV, Meyer TJ. 1983. Photochemistry of $Ru(bpy)_3^{2+}$: solvent effects. *J Am Chem Soc* **105**:5583–5590.
128. Caspar JV, Kober EM, Sullivan BP, Meyer TJ. 1982. Application of the energy gap law to the decay of charge-transfer excited states. *J Am Chem Soc* **104**:630–632.
129. Bixon M, Jortner J. 1968. Intramolecular radiationless transitions. *J Chem Phys* **48**(2):715–726.
130. Freed KF, Jortner J. 1970. Multiphonon processes in the nonradiative decay of large molecules. *J Chem Phys* **52**(12):6272–6291.
131. Nuñez ME, Barton JK. 2000. Probing DNA charge transport with metallointercalators. *Curr Opin Chem Biol* **4**:199–206.
132. Grimm GN, Boutorine AS, Lincoln P, Nordén B, Hélène C. 2002. Formation of DNA triple helices by an oligonucleotide conjugated to a fluorescent ruthenium complex. *ChemBioChem* **3**:324–331.
133. Turro C, Bossmann SH, Jenkins Y, Barton JK, Turro NJ. 1995. Proton transfer quenching of the MLCT excited state of $Ru(phen)_2$-$dppz^{2+}$ in homogeneous solution and bound to DNA. *J Am Chem Soc* **117**:9026–9032.
134. Nair RB, Cullum BM, Murphy CJ. 1997. Optical properties of [$Ru(phen)_2$dppz]$^{2+}$ as a function of nonaqueous environment. *Inorg Chem* **36**:962–965.
135. Nair RB, Murphy CJ. 1998. On the interaction of [$Ru(phen)_2$dppz]$^{2+}$ (dppz=dipyrido[3,2-*a*:2',3'-*c*]phenazine) with different oligonucleotides. *J Inorg Biochem* **69**:129–133.
136. Coates CG, McGarvey JJ, Callaghan PL, Coletti M, Hamilton JG. 2001. Probing the interaction of [$Ru(phen)_2$(dppz)]$^{2+}$ with single-stranded DNA—what degree of protection is required for operation of the "light-switch effect"? *J Phys Chem* **105**:730–735.
137. Önfelt B, Lincoln P, Nordén B. 2001. Enantioselective DNA threading dynamics by phenazine-linked [$Ru(phen)_2$dppz]$^{2+}$ dimers. *J Am Chem Soc* **123**:3630–3637.
138. Friedman AE, Chambron JC, Sauvage J-P, Turro NJ, Barton JK. 1990. Molecular light switch for DNA $Ru(bpy)_2(dppz)^{2+}$. *J Am Chem Soc* **112**:4960–4962.
139. Del Guerzo A, Mesmaeker AK–D. 2002. Novel DNA sensor for guanine content. *Inorg Chem* **41**(4):938–945.

140. Garcia-Fresnadillo D, Boutonnet N, Schumm S, Moucheron C, Mesmaeker AK-D, Defrancq E, Constant JF, Lhomme J. 2002. Luminescence quenching of Ru-labeled oligonucleotides by targeted complementary strands. *Biophys J* **82**:978–987.
141. Del Guerzo A, Mesmaeker AK-D, Demeunynck M, Lhomme J. 1997. Photophysics of bifunctional Ru(II) complexes bearing an aminoquinoline organic unit: potential new photoprobes and photoreagents of DNA. *J Phys Chem B* **101**:7012–7021.
142. Kang JS, Abugo OO, Lakowicz JR. 2002. Dynamics of supercoiled and relaxed pTZ18U plasmids probed with a long-lifetime metal–ligand complex. *J Biochem Mol Biol* **35**(4):389–394.
143. Kang JS, Abugo OO, Lakowicz JR. 2002. Dynamics of supercoiled and linear pTZ18U plasmids observed with a long-lifetime metal–ligand complex. *Biopolymers* **67**:121–128.
144. Lakowicz JR, Malak H, Gryczynski I, Castellano FN, Meyer GJ. 1995. DNA dynamics observed with long lifetime metal–ligand complexes. *Biospectroscopy* **1**:163–168.
145. Malak H, Gryczynski I, Lakowicz JR, Meyer GJ, Castellano FN. 1997. Long-lifetime metal–ligand complexes as luminescent probes for DNA. *J Fluoresc* **7**(2):107–112.
146. Jenkins Y, Friedman AE, Turro NJ, Barton JK. 1992. Characterization of dipyridophenazine complexes of ruthenium (II): the light switch effect as a function of nucleic acid sequence and conformation. *Biochemistry* **31**:10809–10816.
147. Holmlin RE, Stemp EDA, Barton JK. 1998. $Ru(phen)_2dppz^{2+}$ luminescence: dependence on DNA sequences and groove-binding agents. *Inorg Chem* **37**:29–34.
148. Chang Q, Murtaza Z, Lakowicz JR, Rao G. 1997. A fluorescence lifetime-based solid sensor for water. *Anal Chim Acta* **350**:97–104.
149. Guo X-Q, Castellano FN, Li L, Lakowicz JR. 1998. A long-lifetime Ru(II) metal–ligand complex as a membrane probe. *Biophys Chem* **71**:51–62.
150. Anderson CM, Zucker FH, Steitz TA. 1979. Space-filling models of kinase clefts and conformation changes. *Science* **204**:375–380.
151. Grossman SH. 1990. Resonance energy transfer between the active sites of creatine kinase from rabbit brain. *Biochim Biophys Acta* **1040**:276–280.
152. Grossman SH. 1989. Resonance energy transfer between the active sites of rabbit muscle creatine kinase: analysis by steady-state and time-resolved fluorescence. *Biochemistry* **28**:5902–5908.
153. Haran G, Haas E, Szpikowska BK, Mas MT. 1992. Domain motions in phosphoglycerate kinase: Determination of interdomain distance-distributions by site-specific labeling and time-resolved fluorescence energy transfer. *Proc Natl Acad Sci USA* **89**:11764–11768.
154. Holowka D, Wensel T, Baird B. 1990. A nanosecond fluorescence depolarization study on the segmental flexibility of receptor-bound immunoglobulin E. *Biochemistry* **29**:4607–4612.
155. Zheng Y, Shopes B, Holowka D, Biard B. 1991. Conformations of IgE bound to its receptor Fc epsilon RI and in solution. *Biochemistry* **30**:9125–9132.
156. Li L, Szmacinski H, Lakowicz JR. 1997. Long-lifetime lipid probe containing a luminescent metal–ligand complex. *Biospectroscopy* **3**(2):155–159.
157. Li L, Szmacinski H, Lakowicz JR. 1997. Synthesis and luminescence spectral characterization of long-lifetime lipid metal–ligand probes. *Anal Biochem* **244**:80–85.
158. Urios P, Cittanova N. 1990. Adaptation of fluorescence polarization immunoassays to the assay of macromolecules. *Anal Biochem* **185**: 308–312.
159. Thompson RB, Vallarino LM. 1988. Novel fluorescent label for time-resolved fluorescence immunoassay. *SPIE Proc* **909**:426–433.
160. Terpetschnig E, Szmacinski H, Lakowicz JR. 1995. Fluorescence polarization immunoassay of a high molecular weight antigen based on a long-lifetime Ru–ligand complex. *Anal Biochem* **227**:140–147.
161. Youn HJ, Terpetschnig E, Szmacinski H, Lakowicz JR. 1995. Fluorescence energy transfer immunoassay based on a long-lifetime luminescence metal–ligand complex. *Anal Biochem* **232**:24–30.
162. Guo X-Q, Castellano FN, Li L, Lakowicz JR. 1998. Use of a long-lifetime Re(I) complex in fluorescence polarization immunoassays of high-molecular-weight analytes. *Anal Chem* **70**:632–637.
163. Lakowicz JR, Murtaza Z, Jones WE, Kim K, Szmacinski H. 1996. Polarized emission from a rhenium metal–ligand complex. *J Fluoresc* **6**(4):245–249.
164. Brewer RG, Jensen GE, Brewer KJ. 1994. Long-lived osmium (II) chromophores containing 2,3,5,6-tetrakis(2-pyridyl)pyrazine. *Inorg Chem* **33**:124–129.
165. Murtaza Z, Herman P, Lakowicz JR. 1999. Synthesis and spectral characterization of a long-lifetime osmium (II) metal–ligand complex: a conjugatable red dye for applications in biophysics. *Biophys Chem* **80**:143–151.
166. Murtaza Z, Lakowicz JR. 1999. Long-lifetime and long-wavelength osmium (II) metal complexes containing polypyridine ligands: excellent red fluorescent dyes for biophysics and for sensors. *SPIE Proc* **3602**:309–315.
167. Shen Y, Maliwal BP, Lakowicz JR. 2003. Red-emitting Ru(II) metal–ligand complexes. *J Fluoresc* **13**(2):163–168.
168. Sun S-S, Lees AJ, Zavalij PY. 2003. Highly sensitive luminescent metal-complex receptors for anions through charge-assisted amide hydrogen bonding. *Inorg Chem* **42**(11):3445–3455.
169. Duff T, Grübing A, Thomas J-L, Duati M, Vos JG. 2003. Luminescent anion recognition: probing the interaction between dihydrogenphosphate anions and Ru(II) polypyridyl complexes in organic and aqueous media. *Polyhedron* **22**:775–780.
170. Rowe HM, Xu W, Demas JN, DeGraf BA. 2002. Metal ion sensors based on a luminescent ruthenium (II) complex: the role of polymer support in sensing properties. *Appl Spectrosc* **56**(2):167–173.
171. Uppadine LH, Redman JE, Dent SW, Drew MGB, Beer PD. 2001. Ion pair cooperative binding of potassium salts by new rhenium (I) bipyridine crown ether receptors. *Inorg Chem* **40**:2860–2869.
172. Wolfbeis OS, Klimant I, Werner T, Huber C, Kosch U, Krause C, Neurauter G, Dürkop A. 1998. Set of luminescence decay time based chemical sensors for clinical applications. *Sens Actuators B* **51**: 17–24.
173. Sun S-S, Lees AJ. 2000. Anion recognition through hydrogen bonding: a simple, yet highly sensitive, luminescent metal–complex receptor. *Chem Commun* **17**:1687–1688.
174. deSilva AP, Fox DB, Huxley AJM, McClenaghan WM, Roioron J. 1999. Metal complexes as components of luminescent signalling systems. *Coord Chem Rev* **185–186**:297–306.
175. Anzenbacher P, Tyson DS, Jursiková K, Castellano FN. 2002. Luminescence lifetime-based sensor for cyanide and related anions. *J Am Chem Soc* **124**:6332–6233.

176. Montalti M, Wadhwa S, Kim WY, Kipp RA, Schmehl RH. 2000. Luminescent ruthenium (II) bipyridyl-phosphonic acid complexes: pH dependent photophysical behavior and quenching with divalent metal ions. *Inorg Chem* **39**:76–84.
177. Wang K-Z, Gao L-H, Bai G-Y, Jin L-P, 2002. First protein-induced near-infrared fluorescent switch at room temperature of a novel Ru(II) complex. *Inorg Chem Commun* **5**:841–843.
178. Grigg R, Norbert WDJA. 1992. Luminescent pH sensors based on di(2,-2'-bipyridyl)(5,5-diaminomethyl-2,2'-bipyridyl)-ruthenium(II) complexes. *J Chem Soc Chem Commun*, pp 1300–1302.
179. Mack NH, Bare WD, Xu W, Demas JN, DeGraff BA. 2001. An automated approach to luminescence lifetime and intensity titrations. *J Fluoresc* **11**(2):113–118.
180. Licini M, Williams JAG. 1999. Iridium (III) bis-terpyridine complexes displaying long-lived pH sensitive luminescence. *Chem Commun* **18**:1943–1944.
181. Murtaza Z, Chang Q, Rao G, Lin H, Lakowicz JR. 1997. Long-lifetime metal–ligand pH probe. *Anal Biochem* **247**:216–222.
182. Kang JS, Piszczek G, Lakowicz JR. 2002. Enhanced emission induced by FRET from a long-lifetime, low quantum yield donor to a long-wavelenth, high quantum yield acceptor. *J Fluoresc* **12**(1): 97–103.
183. Lakowicz JR, Piszczek G, Kang JS. 2001. On the possibility of long-wavelength long-lifetime high-quantum yield luminophores. *Anal Biochem* **288**:62–75.
184. Maliwal BP, Gryczynski Z, Lakowicz JR. 2001. Long-wavelength long-lifetime luminophores. *Anal Chem* **73**:4277–4285.
185. Castellano FN, Lakowicz JR. 1998. A water-soluble luminescence oxygen sensor. *Photochem Photobiol* **67**(2):179–183.

## PROBLEMS

P20.1. *Effect of Off-Gating on the Background Level*: Figure 20.50 shows the intensity decay of a long-lifetime sensing probe ($\tau_2$) with an interfering autofluorescence of $\tau_1 = 7$ ns.

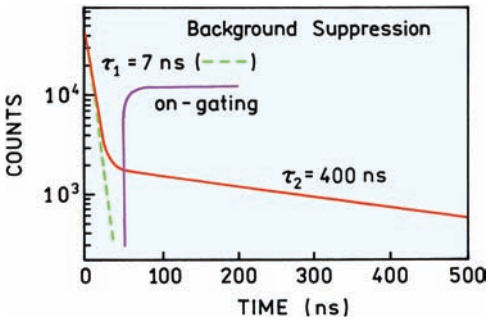


**Figure 20.50**. Intensity decay of a long-lifetime probe having a decay time of 400 ns, with an interfering autofluorescence of 7 ns.

A. The decay time of the long-lifetime component is 400 ns. Confirm this by your own calculations.

B. What are the values of $\alpha_i$ in the intensity decay law? That is, describe $I(t)$ in terms of $\alpha_1 \exp(-t/\tau_1) + \alpha_2 \exp(-t/\tau_2)$.

C. What are the fractional intensities ($f_i$) of the two components in the steady-state intensity measurements?

D. Suppose the detector was gated on at 50 ns, and that the turn-on time is essentially instantaneous in Figure 20.50. Assume that the intensities are integrated to 5 μs, much longer than $\tau_2$. What are the fractional intensities of each component? Explain the significance of this result for clinical and environmental sensing applications. It is recommended that the integrated fractional intensities be calculated using standard computer programs.

P20.2. *Oxygen Bimolecular Quenching Constant for a Metal-Ligand Complex*: The complex of ruthenium with three diphenylphenanthrolines $[Ru(dpp)_3]^{2+}$ displays a long lifetime near 5 μs and has found widespread use as an oxygen sensor. Recently a water-soluble version of the sensor has been synthesized (Figure 20.51).[185] Frequency-domain intensi-

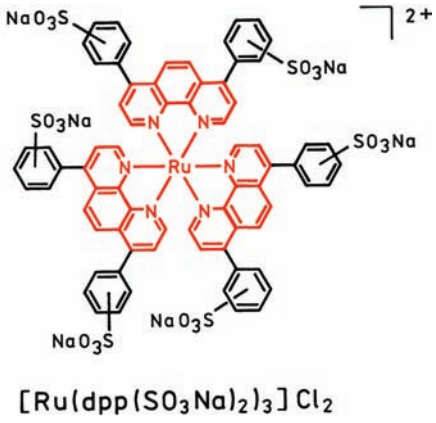


**Figure 20.51**. Structure of a water-soluble MLC used as an oxygen sensor.

ty data for $[Ru(dpp(SO_3Na)_2)_3]Cl_2$ are shown in Figure 20.52. Calculate the oxygen bimolecular quenching constant for this complex. Assume the solubility of oxygen in water is 0.001275 M/atm.

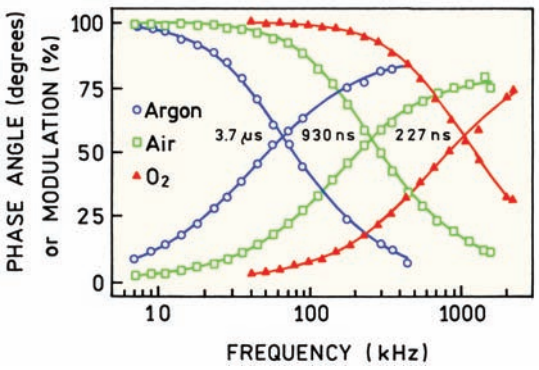


**Figure 20.52**. Frequency-domain intensity decay of $[Ru(dpp)(SO_3Na)_2)_3]Cl_2$ in water, under an atmosphere of argon (o), air (□), or oxygen (▼).